DOI:
10.1016/j.applthermaleng.2021.116623

Thermal and mechanical abuse of electric vehicle pouch cell modules

P. A. Christensen [a, 1], Z. Milojevic [a], M. S. Wise [a], M. Ahmeid [a], P. S. Attidekou [a], W. Mrozik [a], N. A. Dickman [a], F. Restuccia [b], S. M. Lambert [a], and P. K. Das [a]

[a] School of Engineering, Newcastle University, Newcastle upon Tyne, NE1 7RU, UK.
[b] Department of Engineering, King's College London, Strand Building, London, WC2R 2LS, UK.
[1] Corresponding author.

Abstract

This paper reports thermal (burner) and mechanical (blunt trauma and nail penetration) abuse experiments on electric vehicle lithium ion modules comprising eight 56.3Ah lithium nickel manganese cobalt (NMC) pouch cells. The aim of project part of which is described in this paper was to study the problem of thermal runaway in lithium ion batteries under different abuse conditions and at different SOC and to bridge the current gap in the literature between cell level studies and research at pack and system level. These experiments were part of an ongoing research programme leading up to studies at pack and system level. The responses of the cells to the various forms of abuse were monitored with optical and thermal cameras, thermocouples and by measuring cell voltage. Draeger gas sensors were also employed where possible. The nail penetration experiments were carried out at (nominally) 96.5%, 75% and 50% SOC, and at 96.5% SOC as a function of penetration location: the experiments strongly suggest that low SOC is as hazardous as high SOC, in contrast to a general perception in the literature, as the likely hazards are simply different and include the possibility of violent vapour cloud explosion. Thus, in all experiments, the first obvious indication of thermal runaway was the ejection of white vapour: if this ignited, the obvious hazard was that of fire. If, however, the vapour did not ignite, it posed an entirely different hazard in terms of high toxicity and the potential for a violent vapour cloud explosion: this is the first mention of such a phenomenon linked to lithium ion batteries in the academic literature. The experiments showed that cell voltage cannot be employed as a reliable warning of thermal runaway. Finally, the data obtained support a wholly novel theory, yet to be adopted across the community, in which thermal runaway can involve the direct solid-state electrochemical reaction between anode and cathode at temperatures ≥ 250 ˚C following venting of the electrolyte.

Keywords

Vapour Cloud explosion; lithium ion battery; abuse; thermal runaway; modules; SOC.

Nomenclature

Abbreviation	Meaning
APS	Arizona Public Services
BMS	Battery Management System

This is the accepted version of this paper. Paper can be referenced as:
P. Christensen, Z. Milojevic, M.S. Wise, M. Ahmeid, P.S. Attidekou, W. Mrozik, N.A. Dickman, F. Restuccia, S.M.Lambert, P.K. Das. *Thermal and mechanical abuse of electric vehicle pouch cell modules*, Applied Thermal Engineering, 2021. https://doi.org/10.1016/j.applthermaleng.2021.116623

DAQ	Data Acquisition unit
EV	Electric Vehicle
FSC	Fire Services College, Moreton-in-Marsh
HCl	Hydrogen chloride
HCN	Hydrogen cyanide
HEV	Hybrid Electric Vehicle
HF	Hydrogen fluoride
IET	Immediate Effects Threshold
ISC	Internal Short Circuit
FLET	First Lethal Effects Threshold
LFP	Lithium iron Phosphate (active cathode material)
LiB	Lithium ion Battery
LiBESS	Lithium ion Battery Energy Storage System
LiFSI	Lithium bis(fluorosulfonyl)imide
LMO	Lithium Manganese Oxide (active cathode material)
NMC	Lithium Nickel Manganese Cobalt oxide (active cathode material)
OCV	Open Circuit Voltage
OEM	Original Equipment Manufacturer
PET	PolyEthylene Terephthalate
PVDF	PolyVinylidene DiFluoride
SEI	Solid Electrolyte Interface
SEM	Scanninf Electron Microscopy
SOC	State Of Charge
SOH	State Of Health

1.0 Introduction

Lithium ion batteries (LiBs) are a major boon for humankind, not least because they are essential for the decarbonisation of this planet due to their ability to store high electrical energy densities from wind, wave and solar generators. Hopefully this should also reduce geopolitical tensions as we move away from oil as the energy vector. However, the benefits of LiBs come with the demand, common to all new technologies, that their risks and hazards are fully understood and addressed: “Sustainable energy sources are rapidly proliferating and very much needed, and energy storage is a critical component of it. This is a global fire protection problem, and we all have work to do in support of the safe evolution of this technology." [1]. In essence, until the mid-late 2000s, the primary function of LiBs was to power personal electronic devices: however, since ca. 2007 the scale of their application has increased dramatically[2]: initially in 10s to 100 kWh electric vehicle (EV) battery packs, and then in MW industrial lithium ion battery energy storage systems (LiBESS). Economies of scale have pushed the actual energy densities of such systems towards the theoretical values and sometimes explosive failures have taken place on land and sea [3 - 5].

This is the accepted version of this paper. Paper can be referenced as:
P. Christensen, Z. Milojevic, M.S. Wise, M. Ahmeid, P.S. Attidekou, W. Mrozik, N.A. Dickman, F. Restuccia, S.M.Lambert, P.K. Das. *Thermal and mechanical abuse of electric vehicle pouch cell modules*, Applied Thermal Engineering, 2021. https://doi.org/10.1016/j.applthermaleng.2021.116623

The ignition or explosion of LiBs is generally caused by abuse – either physically or functionally: lithium ion batteries don't die- they are murdered. Abuse is generally due to heating, penetration, blunt trauma or overcharge caused by e.g. (see [2][3][6] and references therein): poor ventilation, debris on the road penetrating the battery pack of an EV [2][7], accidental dropping of a LiB or EV crash and Battery Management System (BMS) failure [2][3], respectively. Abuse can result in the venting of toxic and flammable/explosive gases including HF [8 -12], fire and explosion. The ignition of encased LiBs, e.g. in EV battery packs, is very difficult to deal with as it is usually impossible to access the root of the fire with water, and large LiB systems tend to burn for longer and have the added hazards of re-ignition hours, days or even weeks after the initial incident as well as stranded electrical energy [3][6][8][13]. Hence LiB fires pose a wholly novel challenge to first responders who are on a very steep learning curve.

Of particular note is the explosion at the Surprise, Arizona LiBESS owned by Arizona Public Services (APS) in April 2019 [14 – 17] which resulted in eight firefighters and one police officer being transported to local hospitals. Four firefighters and the police officer were transported for observation due to detectable levels of HCN in their protective clothing and the officer's uniform. Four first responders were injured[16] and two of the firefighters required numerous surgeries to repair broken bones, etc., and their face masks were blown off during the explosion[17]. One firefighter was recovered about 55 feet away from the building and the other firefighter was located about 73 feet away from the building: the explosion blew both of them underneath an industrial grade chain length fence and the force of the explosion distorted the steel container. The explosion took place when the door to the steel container was opened some three hours after the BMS of the LiBESS first recorded a thermal event [17]. The report on the incident prepared by DNV GL for APS identified lithium metal dendrite formation as one of the key factors in the explosion[14]: this was contested by the manufacturer of the lithium ion cells, LG Chem, in the report commissioned in response to the DNV GL report [15], on the basis of the fact that the deposits specified in the DNV GL report were not electronically conducting. However, the manufacturers did state that the deposits were pyrophoric, as would be expected of lithium metal. Neither report addressed the key question of why lithium metal, in whatever form, was deposited on the anode as such deposition is generally associated with low temperature operation or overcharging.

The Surprise explosion followed 23 fires involving LiBESS in South Korea, the report on which has not been made public [18] but the fires have been blamed on faulty batteries[19]. More recently, a BESS

This is the accepted version of this paper. Paper can be referenced as:
P. Christensen, Z. Milojevic, M.S. Wise, M. Ahmeid, P.S. Attidekou, W. Mrozik, N.A. Dickman, F. Restuccia, S.M.Lambert, P.K. Das. *Thermal and mechanical abuse of electric vehicle pouch cell modules*, Applied Thermal Engineering, 2021. https://doi.org/10.1016/j.applthermaleng.2021.116623

exploded at the Nathan campus of Griffith University in Brisbane, Australia[20][21] on 17 March 2020: this incident is noteworthy as the lithium ion cells involved employed lithium iron phosphate (LFP) cathodes, which are generally considered to be the safest and most stable [2][3] and references therein. It was also the first incident of its kind in Australia. The cause of the fire and explosion has been stated as having been an internal short circuit [20][21].

The ignition of lithium ion cells is due to thermal runaway, where heat produced in the cell is dissipated more slowly than it is generated by the abuse, and the various processes leading up to thermal runaway and the subsequent events have been extensively researched (see [22] and references therein) as has the thermal management of LiBs[23][24] However, the majority of papers in the literature are focussed on individual cells, usually cylindrical 18650 format, and there is very little research on larger format prismatic or pouch cells or modules [24], in particular, that includes the composition of the vapours and fumes emitted from these when abused. Furthermore, despite the prominence of NMC cathodes in LiBs, research on the abuse of NMC pouch or prismatic cells and the gases released remains limited [25]. Experiments have been carried out on full battery packs by Li et. al. [26] and Sturk et. al. [8], but the latter does not include any data on the fumes evolved and the former provides very limited information on the battery pack ignition experiment.

It is generally considered that once electric vehicle packs reach ca. 80% state-of-health (SOH: i.e. the available capacity is 80% of the new pack) they are no longer fit-for-purpose in EVs, but still have significant capacities and hence can be repurposed [27] and cells, modules and battery packs from electric vehicles are now freely available to be bought by consumers online. This has caused widespread concern from regulators, first responders and even the OEMs, who fear the potential for reputational damage, as such pack components are being employed in home built, domestic LiBESS and the installation of commercial and domestic BESS is largely unregulated [28]. Furthermore, such domestic systems can be installed in homes etc without the local fire services being aware and hence pose a major potential hazard in the event of a fire or BMS failure.

It is important to note that the instances of fires involving large lithium ion batteries such as in EVs, ships & ferries and LiBESS remain insignificant at the present time, however, the first explosion and fire involving a (20MW) LiBESS on British soil occurred in September 2020 on Merseyside [29]: interestingly, the latter LiBESS had been in service for around the same length of time (ca. 2 years) as the Surprise LiBESS. In addition, the uptake of LiB technology is set to increase dramatically over the next decade or so: for

This is the accepted version of this paper. Paper can be referenced as:
P. Christensen, Z. Milojevic, M.S. Wise, M. Ahmeid, P.S. Attidekou, W. Mrozik, N.A. Dickman, F. Restuccia, S.M.Lambert, P.K. Das. *Thermal and mechanical abuse of electric vehicle pouch cell modules*, Applied Thermal Engineering, 2021. https://doi.org/10.1016/j.applthermaleng.2021.116623

example, the UK Prime Minister has announced a ban on the sale of internal combustion engine vehicles (including hybrids) from 2035 in order to drive the uptake of EVs, and the global market in LiBs is predicted to double to $7bn over the next 5 years [30]. Simple probability considerations suggest that first responders are increasingly likely to face incidents involving large LiBs. A recent meta-review of battery fire literature shows that understanding of thermal runaway (at the component, cell and pack levels) is crucial to drive improvements, integration, and harmonization of LiB safety [6]. This paper aims to bridge some of that gap for larger scale systems i.e. modules and module stacks, the latter representative of domestic lithium ion battery energy storage systems.

This paper reports abuse experiments conducted using Envision-AESC modules (8 x 53.8 Ah NMC pouch cells) in collaboration with Envision-AESC, the London Fire Brigade and Draeger. Observers included personnel from a number of first responder and government organisations, and industry. The aim of the work reported in this paper was to investigate and analyse the thermo-physical events occurring during the abuse of LIB modules, as well as stacks of modules representing domestic BESS, in order to understand thermal runaway conditions in these larger systems. These preliminary studies are intended to provide the foundation for future pack- and system- level research. This will benefit the academic community, by having a better understanding of significantly understudied topics such as thermal propagation between cells, time to ignition, size and length of flame flaring during the highly transient combustion phases of the module, and emission characteristics. Most importantly, results from the project can then be used in informing the standard operating procedures of first responders.

2.0 Experimental

It should be noted that the nail penetration experiments were conducted using forces well in excess of industry testing norms.

The experiments were conducted at the DNV GL site at RAF Spadeadam and the Fire Services College at Moreton-in-Marsh. Seven experiments were conducted at the DNV GL site starting with a gas burner, followed by three nail penetrations at various locations on the module surface and two overcharge experiments, one involving a single module and the last experiment a stack of three modules. Three experiments were conducted at the FSC site, two nail penetrations at different SOC and one overcharge experiment involving five modules. For space considerations, this paper reports the results only of the

This is the accepted version of this paper. Paper can be referenced as:
P. Christensen, Z. Milojevic, M.S. Wise, M. Ahmeid, P.S. Attidekou, W. Mrozik, N.A. Dickman, F. Restuccia, S.M.Lambert, P.K. Das. *Thermal and mechanical abuse of electric vehicle pouch cell modules*, Applied Thermal Engineering, 2021. https://doi.org/10.1016/j.applthermaleng.2021.116623

burner and nail penetration at fixed location experiments. The data from the remaining experiments (nail penetration at various locations and overcharge) will be reported in later papers.

2.1 The lithium ion modules

The modules employed were supplied by Envision-AESC, were the same as those employed in the 2018 Nissan Leaf and consisted of eight 56.3 Ah pouch cells, see Figures S1(a) to (c), connected as shown in Figure S1(c). The modules were unused.

The specifications of the modules are summarised in Table 1. All the modules employed were manufactured in the UK and had been stored for some months but were unused.

Chemistry	**$LiNiMnCoO_2$ (NMC)**
Number of cells	8
Cell capacity /Ah	56.3
Cell nominal voltage /V	3.65
Cell voltage range /V	2.5 – 4.2
Module capacity /Wh	1640
Module dimensions (L x W x H) /mm	300 x 222 x 68
Module mass /kg	8.5

Table 1. Specifications of the modules. The anodes were graphite.

2.2 The module mounting framework

The frame employed to mount the modules and allow nail penetration and burner ignition is shown in Figure S2. The frame was 1710 mm long x 900 mm wide x 200 mm high and was manufactured & welded together from 50mm, square box section mild steel, 3 mm thick. It had a 1500 m long pivot arm, made from 40 mm x 40 mm x 6 mm "T" section mild steel, and pivoted on a 25 mm dia. shaft and bearings. The hammer was a 100 mm diameter x 75 mm long mild steel bar, weighing ca. 6 kg. The piercing pin (nail) was 100 mm long and 12 mm diameter silver steel (type 01 carbon tool steel), with a 30˚ tapered point to the end, which protruded 75 mm from the flat face of the hammer. The hammer arm assembly was held in place by a 10 mm dia. safety release pin which was attached to a chain & cord for release at a safe distance. The piercing pin was held in place with an M6 socket head bolt to allow easy replacement or removal from the hammer.

This is the accepted version of this paper. Paper can be referenced as:
P. Christensen, Z. Milojevic, M.S. Wise, M. Ahmeid, P.S. Attidekou, W. Mrozik, N.A. Dickman, F. Restuccia, S.M.Lambert, P.K. Das. *Thermal and mechanical abuse of electric vehicle pouch cell modules*, Applied Thermal Engineering, 2021. https://doi.org/10.1016/j.applthermaleng.2021.116623

The modules were clamped in position using M8 steel studding (with nuts and washers) of various lengths, appropriate to the number of modules, using clamping plates made from 25 mm wide x 6 mm thick mild steel plate.

The burner was attached to a 30 mm diameter, mild steel tube to protect the gas pipe with a chain attached to allow retraction from a safe position. Mild steel trays, 1.5 mm thick, allowed the burner to be retracted smoothly from beneath the modules.

2.3 Thermal imaging

Two thermal imaging FLIR A655sc 25º cameras were employed in the experiments at the DNV GL site at RAF Spadeadam. These were not employed in the experiments at the Fire Services College (FSC) due to concerns over potential damage. The FLIR cameras allowed the temperature of the surface of the modules to be recorded at a rate of 1 Hz. In addition, to obtain precise temperature measurements and to decrease reflections, black matt spray paint was applied on the module surface with emissivity value of 0.9. Type K thermocouples were used to facilitate the calibration of the thermal cameras. An ISGX380 thermal camera supplied by the Northamptonshire Fire Service was employed during the experiments at the FSC.

2.4 Optical Imaging

For the experiments at the DNV GL site, two high-speed GoPro Hero 7 black cameras were employed which were able to record video images at 240 frames per second, at a resolution of 1280 x 720 pixels. Whilst these cameras provide a lower frame rate than is achievable with other commercially available equipment this is offset by the longer video recording time achievable and the fact that the GoPro cameras are waterproof. At the FSC, a Vmotal GSV8560 camera was employed, recording video images at 30 frames per second at a resolution of 2688 x 1520 pixels.

The arrangement of the thermal and video optical cameras at the DNV GL and FSC sites are shown in Figures S3(a) and (b), respectively.

2.5 Flame length and area calculations

With respect to the DNV GL experiments, the images from the optical cameras offered an insight into the behaviour of the flames from the modules on ignition, and were used to measure the total areas of flame observed from both camera angles, areas that can be used to quantify peaks in heat release, thermal

This is the accepted version of this paper. Paper can be referenced as:
P. Christensen, Z. Milojevic, M.S. Wise, M. Ahmeid, P.S. Attidekou, W. Mrozik, N.A. Dickman, F. Restuccia, S.M.Lambert, P.K. Das. *Thermal and mechanical abuse of electric vehicle pouch cell modules*, Applied Thermal Engineering, 2021. https://doi.org/10.1016/j.applthermaleng.2021.116623

propagation between cells, and characteristics of the flames as a function of time. The optical images from both cameras (front, HS camera 1, and back, HS camera 2, locations) were used to calculate maximum flame lengths as a function of time, and the details are presented in Figure S4. Figures S5 and S6, and the accompanying text, describes the method by which a common timeline was established.

2.6 Thermocouples and voltage monitoring

Type K thermocouples (temperature range 0 – 700°C) were employed with long (10 m) leads. These were monitored along with cell voltages using an Agilent 34970A Data Acquisition unit (DAQ). The thermocouples were cemented in place using Omega CC high temperature cement.

2.7 Gas detection

The gas sensors employed were supplied by Draeger and the specifications are summarised in Table 2. The XXS Nitrogen Dioxide sensor is also sensitive to HCN: as a guide, 60 ppm of HCN will give a reading of ≤ +/- 10ppm of NO_2 on the device. The XXSHCl sensor used is reactive to HCl and HF, along with other gases. The device used in these experiments was setup and calibrated for the detection of HCl and as such there was cross sensitivity to HF. As a guide, HF will give a reading reduced by a factor of 0.66 when shown on a HCl-calibrated device. For example, 10ppm of HF will result in a displayed value of 6.6ppm HCl.

Device / Sensor	**Part Number**	**Maximum concentration /ppm**	**Serial Numbers**
XAM5000	8320000		0379, 0065, 0111
XXS CO	6810882	2000	
XXS NO_2	6810884	50	
XXS SO_2	6810885	100	
XAM5100	8322750		0006, 0007, 0133
XXSHCl	6809140	30	

Table 2. The specifications of the Draeger gas sensors.

The location of the DNV GL site in RAF Spadeadam was fully exposed to the elements and the prevailing wind repeatedly varied in direction, rendering the use of gas sensors of little value, although they did alarm during the various experiments suggesting the production of the various gases specified. This problem was rectified to some extent during the experiments at the Fire Services College as these were conducted in a

This is the accepted version of this paper. Paper can be referenced as:
P. Christensen, Z. Milojevic, M.S. Wise, M. Ahmeid, P.S. Attidekou, W. Mrozik, N.A. Dickman, F. Restuccia, S.M.Lambert, P.K. Das. *Thermal and mechanical abuse of electric vehicle pouch cell modules*, Applied Thermal Engineering, 2021. https://doi.org/10.1016/j.applthermaleng.2021.116623

standard shipping container, although the positioning of the cameras as well as the gas sensors had to take into account possible damage from the ignition of the modules. Figure S7 shows the location of the sensors in the Fire Services College experiments: the lower sensors were ca. 1 m above the floor of the container and the higher sensors were 2 m above. In the text below, sensor positions are identified by the letter L followed by the position: e.g. L1 – L6.

2.8 The experiments

The experiments conducted at the DNV GL and FSC sites are summarised in Tables 3 and 4. The experiments discussed in detail below are marked with *.

Experiment number	Experiment
1*	Burner
2*	Nail penetration between tabs
3	Nail penetration middle
4	Nail penetration middle opposite end to tabs
5*	Blunt trauma
6	Single module overcharge
7	Single module overcharge, middle of 3-module stack

Table 3. The experiments carried out at the DNV GL site in RAF Spadeadam

Experiment number	Experiment
1*	Nail penetration between tabs: 75% SOC
2*	Nail penetration between tabs: 50% SOC
3	Single module overcharge, in 5-module stack

Table 4. The experiments carried out at the Fire Services College

2.8.1 The experiments conducted at the DNV GL site

Unless otherwise stated, prior to the experiment, the modules were charged such that the voltage across each of the four parallel pairs was 4.15V corresponding to 96.5% SOC according to the manufacturer's charge curve.

The voltages of each quartet of cells, which were arranged in two parallel pairs see Figure 1, were monitored and will be referred to as V_1 and V_2 in the text below.

This is the accepted version of this paper. Paper can be referenced as:
P. Christensen, Z. Milojevic, M.S. Wise, M. Ahmeid, P.S. Attidekou, W. Mrozik, N.A. Dickman, F. Restuccia, S.M.Lambert, P.K. Das. *Thermal and mechanical abuse of electric vehicle pouch cell modules*, Applied Thermal Engineering, 2021. https://doi.org/10.1016/j.applthermaleng.2021.116623

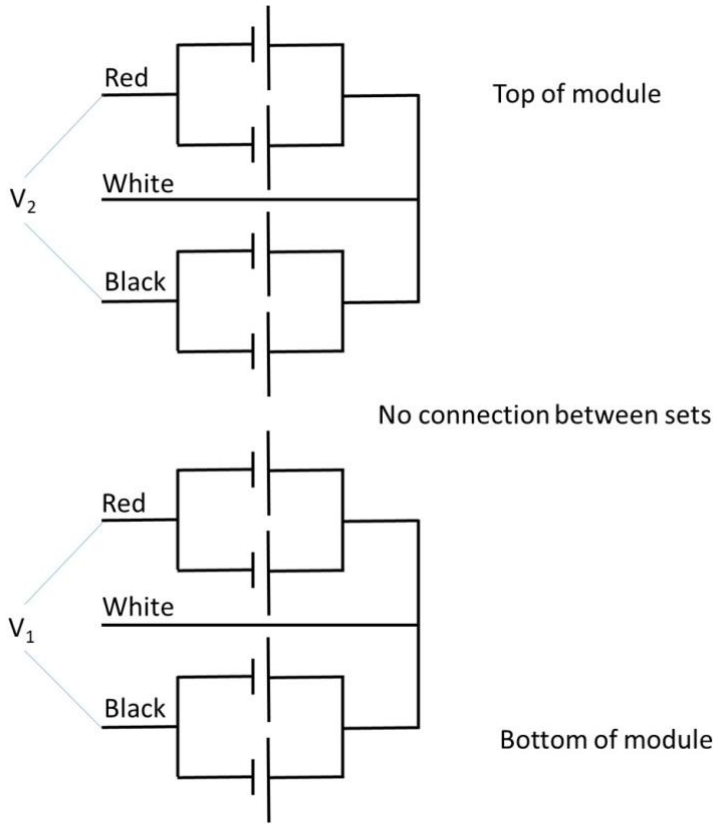

Figure 1. Schematic showing the wiring of the modules and the cell voltages monitored during the experiments at the DNV GL site.

In experiment 1, a propane gas burner was placed directly below the module. Experiments 2 to 4 were nail penetration at different locations on the module, see Figure S8.

In the nail penetration and blunt trauma experiments, a metal hammer was employed which was held upright using a metal pin which was withdrawn using a nylon cord. In the nail penetration experiments, the hammer was fitted with a 12 mm diameter carbon tool steel nail which protruded 75 mm from the hammer base. In the blunt trauma tests a module was mounted at an angle of ca. 15˚ from the horizontal on the frame such that the edge of the hammer (without nail) would strike the middle of the module. A 20 kg metal plate was added to the rear of the hammer to increase the force of impact. Despite dropping the hammer and added metal plate on the module twice, there was no discernible effect and hence these experiments are not dealt with further in this paper.

In all the experiments carried out at the DNV GL site, thermocouples were mounted in the middle of the top and underside faces of the modules and are referred to as TC_{top} and TC_{under} in the discussion below.

This is the accepted version of this paper. Paper can be referenced as:
P. Christensen, Z. Milojevic, M.S. Wise, M. Ahmeid, P.S. Attidekou, W. Mrozik, N.A. Dickman, F. Restuccia, S.M.Lambert, P.K. Das. *Thermal and mechanical abuse of electric vehicle pouch cell modules*, Applied Thermal Engineering, 2021. https://doi.org/10.1016/j.applthermaleng.2021.116623

2.8.2 Experiments conducted at the Fire Services College

Two penetration experiments at 50% SOC and 75% SOC were conducted at the Fire Services College (FSC), with penetration at the top middle, between the tabs, as in experiment 2 at the DNV GL site. To guarantee the module being penetrated was at a certain SOC level, the constant current constant voltage protocol (CCCV) was applied using a HCP-1005 potentiostat from Bio-logic. During the experiments, the voltages of the penetrated modules were monitored as shown in Figure 2.

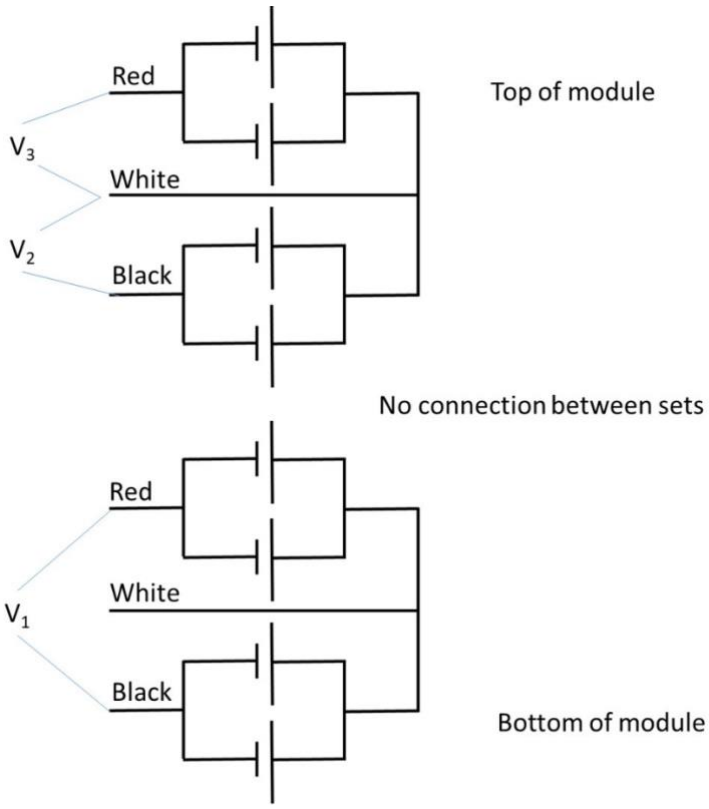

Figure 2. Schematic showing the wiring of the modules and the cell voltages monitored during the experiments at the FSC.

3.0 Results

3.1 DNV GL Site experiment 1, burner.

Stills from the video camera located in front of the module are shown in Figures 3(a) – (c). The burner was moved under the module 27 s into the experiment (i.e. 27 s from when the GoPro cameras were switched on). Smoke was observed 70 s into the experiment (Figure 3(a)), followed by small flames 73 s in (Figure 3(b)). After 106 s the burner was removed and 130 s from the start, flare-like flames were observed to issue from the modules on the side opposite to the connectors (Figure 3(c)), as expected, as the pouch cells are designed to vent from the bottom of the cell (i.e. furthest away from the tabs) on ignition.

This is the accepted version of this paper. Paper can be referenced as:
P. Christensen, Z. Milojevic, M.S. Wise, M. Ahmeid, P.S. Attidekou, W. Mrozik, N.A. Dickman, F. Restuccia, S.M.Lambert, P.K. Das. *Thermal and mechanical abuse of electric vehicle pouch cell modules*, Applied Thermal Engineering, 2021. https://doi.org/10.1016/j.applthermaleng.2021.116623

(a)

(b)

<u>This is the accepted version of this paper. Paper can be referenced as:</u>
P. Christensen, Z. Milojevic, M.S. Wise, M. Ahmeid, P.S. Attidekou, W. Mrozik, N.A. Dickman, F. Restuccia, S.M.Lambert, P.K. Das. *Thermal and mechanical abuse of electric vehicle pouch cell modules*, Applied Thermal Engineering, 2021. https://doi.org/10.1016/j.applthermaleng.2021.116623

(c)

Figure 3. Stills from the video images: (a) 70s, (b) 73s and (c) 130s from the start of the first experiment at the DNV GL site.

The sequential loss of the cells can be seen in the plots of flame lengths calculated using the images from the two GoPro cameras, see Figure 4, and more clearly in the plots of flame areas in Figure 5(a) where 7 separate peaks were observed in a span of 3 minutes, suggesting distinct thermal propagation between the cells at each peak.

The flames visible in Figure 3(a) were external to the module and were due to the burner. In (b), flames began to be generated from the module in addition to the burner. In (c), with the burner completely removed, all flames were being generated from the module itself and flare-like flames were observed from the module, with flame lengths as shown in Figure 4: the latter shows six spikes due to flares: i.e. less clearly defined than the flame areas in Figure 5(a).

Figures 5(b) show plots of the DAQ data recorded during experiment 1 as well as the temperature of the module at the location shown in the inset to Figure 5(b) obtained from the thermal images ("IR Temp") and

This is the accepted version of this paper. Paper can be referenced as:
P. Christensen, Z. Milojevic, M.S. Wise, M. Ahmeid, P.S. Attidekou, W. Mrozik, N.A. Dickman, F. Restuccia, S.M.Lambert, P.K. Das. *Thermal and mechanical abuse of electric vehicle pouch cell modules*, Applied Thermal Engineering, 2021. https://doi.org/10.1016/j.applthermaleng.2021.116623

the flame areas calculated from the image processing of the optical images taken by the GoPro cameras. As can be seen from Figure 5(b), the IR temperature increased immediately as the burner was moved beneath

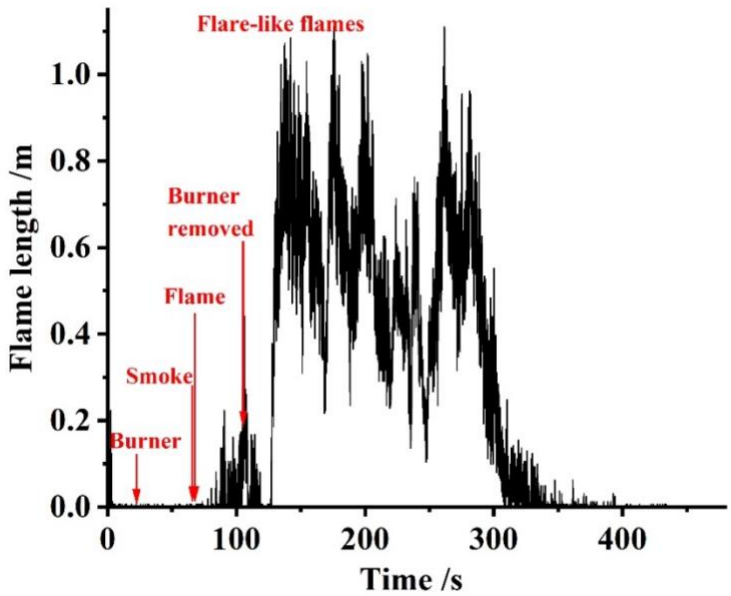

Figure 4. Flame lengths calculated from the burner experiment, experiment 1, at the DNV GL site. See text for details.

the module, rising steadily until ca. 2.42 minutes after which it increases very rapidly (at ca. 98 ˚C s^{-1}) signalling thermal runaway. The camera was calibrated to operate over the ranges -40 to 150°C and 100 to 650°C, and hence flatlined when the temperature reached the top of its range: subsequently, the temperature recorded by the thermal camera decreased after ca. 6 minutes to ca. 400 ˚C, and this coincided with a lack of flames around the region monitored. The thermocouple temperature lagged behind that of the IR by ca. 2 minutes, showing little or no increase until ignition occurred and the production of the flare-like flame, after which it increased to ca. 275˚C for ca. 1 minute before increasing again to 300 – 350 ˚C: the unstable nature of the response reflecting the influence of the flames. From Figures 5(a) and (b) it can be seen that the voltages of the top two parallel pairs of cells in the module collapsed in two clear steps once the temperature on the top face of the module reached ca. 275 ˚C (unfortunately, the monitoring of the output voltage from the lower quartet of cells failed): these steps are clear in Figure S9 which shows the first derivative of the voltage: the voltage collapsed rapidly (ca. 42 and 55 V min^{-1}) in both steps. The temperature registered by

This is the accepted version of this paper. Paper can be referenced as:
P. Christensen, Z. Milojevic, M.S. Wise, M. Ahmeid, P.S. Attidekou, W. Mrozik, N.A. Dickman, F. Restuccia, S.M.Lambert, P.K. Das. *Thermal and mechanical abuse of electric vehicle pouch cell modules*, Applied Thermal Engineering, 2021. https://doi.org/10.1016/j.applthermaleng.2021.116623

the thermal camera rose and then remained at ca. 250 ˚C before increasing rapidly as thermal runaway and ignition took place: this may be due to the collapse of the ceramic-coated separators between the cells [3][31][32]. As can be seen from Figure 5(a), the voltage of the top quartet of cells was maintained for a significant time whilst the module was venting flare-like flames: it does not seem unreasonable to postulate

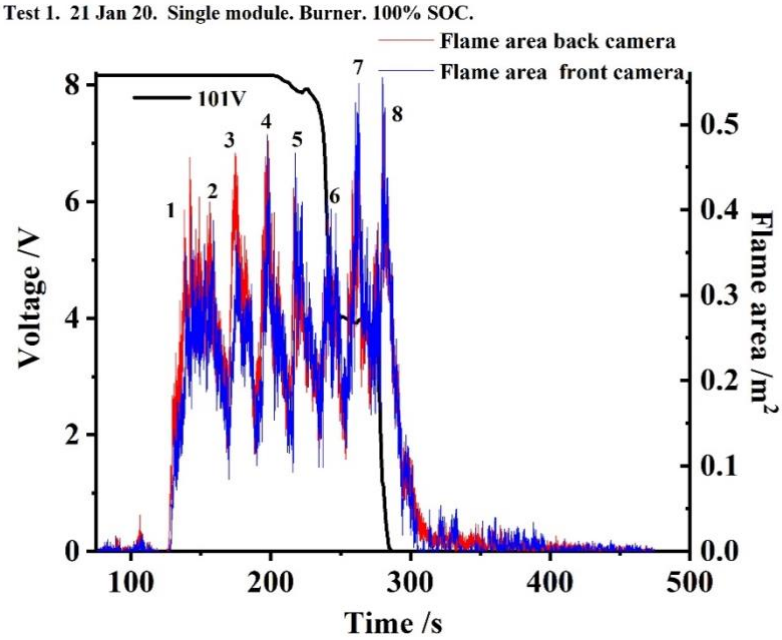

(a)

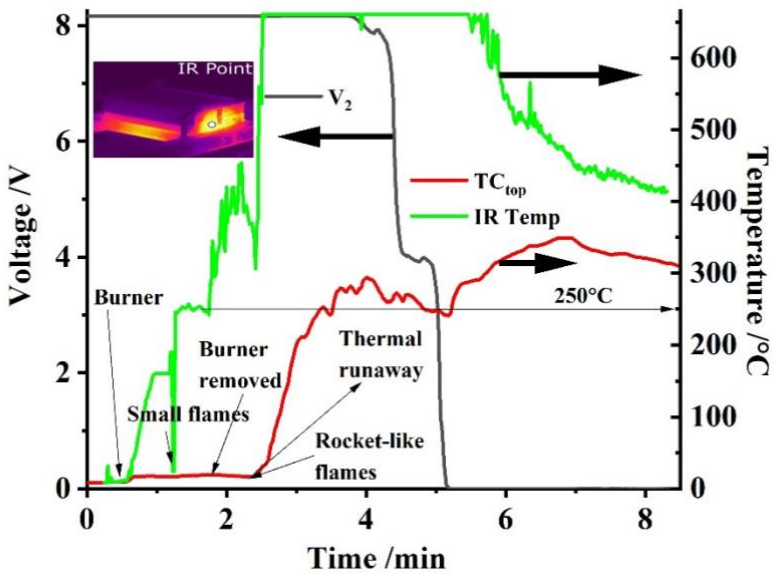

(b)

This is the accepted version of this paper. Paper can be referenced as:
P. Christensen, Z. Milojevic, M.S. Wise, M. Ahmeid, P.S. Attidekou, W. Mrozik, N.A. Dickman, F. Restuccia, S.M.Lambert, P.K. Das. *Thermal and mechanical abuse of electric vehicle pouch cell modules*, Applied Thermal Engineering, 2021. https://doi.org/10.1016/j.applthermaleng.2021.116623

Figure 5. The DAQ and thermal camera data recorded during the burner experiment, experiment 1, at the DNV GL site and the flame areas calculated from the optical videos. The location employed for thermal camera temperature is shown on the inset. (a) cell voltage and flame areas, and (b) cell voltage, thermocouple and thermal imaging data.

that the flares between 125 s and 233 s were due to the lower quartet of cells sequentially igniting after which one cell of one of the remaining parallel pairs ignited with a minor loss of voltage followed by the second of the same pair, causing the voltage to decrease by 50%: this process was then repeated. The maintenance of the cell voltage well after the ignition of the module suggests that, in contrast to reports in the literature, a drop in cell voltage cannot reliably be employed as an early warning of thermal runaway [32].

As can be seen from Figure 5(b), the module remained hot after the last cell ignition and it was generally observed that the module carcasses remained at temperatures significantly above 300 ˚C for over 40 minutes after the fires had ceased, and hence were still potential ignition sources.

3.2 Nail penetration experiments

3.2.1 DNV GL site experiment 2

Experiment 2 involved nail penetration in the middle of the side of the module nearest the module terminals and hence essentially between the connecting tabs of the pouch cells.

Figures 6(a) – (k) shows stills from the GoPro videos taken (a) at nail piercing and (b) – (d) 4.17ms, 16.68ms, 66.72ms and 0.233s after penetration. Figures (e) – (i) were taken 0.54s, 9.48s, 9.50s, 13.42 and 18.05s, respectively, after the image taken in (a).

In Figure 6(a), the nail is just touching the module case whereas ca. 4.17ms later, see (b), it had penetrated sufficiently deeply into the module to significantly deform the case before it bounced up again, see (c), albeit without the nail coming free: it then moved down into the module again such that the hammer touched the casing, (d), this time without deformation. As the nail protruded 75 mm from the hammer and the modules are 68 mm deep, the deformation of the module is clear in Figure 7(b) and there was no apparent bulging of the module, this suggests that all cells were penetrated in the first 4.17ms. This supposition was supported by visual inspection of the module carcass which showed a clear exit hole on the underside of the

This is the accepted version of this paper. Paper can be referenced as:
P. Christensen, Z. Milojevic, M.S. Wise, M. Ahmeid, P.S. Attidekou, W. Mrozik, N.A. Dickman, F. Restuccia, S.M.Lambert, P.K. Das. *Thermal and mechanical abuse of electric vehicle pouch cell modules*, Applied Thermal Engineering, 2021. https://doi.org/10.1016/j.applthermaleng.2021.116623

module, see Figure S10. When the hammer bounced back and the nail partially retraced, it may not have then penetrated again fully.

The subsequent images in the figure highlight the stages generally observed during all the abuse experiments performed on the Envision-AESC modules, as well as reflecting the literature of LiB abuse experiments in general. Thus: Figures 6(e)-(g) the initial evolution of dense, white vapour starting with a wisp immediately after penetration, then (g) & (h) ignition of the vapour to produce much thinner fumes, followed by (i) flare-like flames. Once all the electrical energy was expended, the fire resembled that from burning plastic with smoky flames and thin black smoke.

(a)

(b)

This is the accepted version of this paper. Paper can be referenced as:
P. Christensen, Z. Milojevic, M.S. Wise, M. Ahmeid, P.S. Attidekou, W. Mrozik, N.A. Dickman, F. Restuccia, S.M.Lambert, P.K. Das. *Thermal and mechanical abuse of electric vehicle pouch cell modules*, Applied Thermal Engineering, 2021. https://doi.org/10.1016/j.applthermaleng.2021.116623

(c)

(d)

(e)

(f)

This is the accepted version of this paper. Paper can be referenced as:
P. Christensen, Z. Milojevic, M.S. Wise, M. Ahmeid, P.S. Attidekou, W. Mrozik, N.A. Dickman, F. Restuccia, S.M.Lambert, P.K. Das. *Thermal and mechanical abuse of electric vehicle pouch cell modules*, Applied Thermal Engineering, 2021. https://doi.org/10.1016/j.applthermaleng.2021.116623

(g) *(h)*

Figure 6. Stills from the GoPro videos taken during experiment 2 at the DNV GL site: taken (a) at nail piercing and (b) – (e) 4.17ms, 16.68ms, 66.72 ms and 233.52 ms after penetration. Figures (f) – (i) were taken 0.54s, 9.50s, 13.42 and 18.05s, respectively, after the image taken in (e).

The evolution of white "smoke" or vapour has been observed previously [11] but its significance has been overlooked. From a first responder perspective, it could be mistakenly, and dangerously, attributed to steam especially as it re-appears if a burning cell is extinguished. In fact, as the white vapour has flammable and toxic components (see below), some of which are heavier than air and which include vaporised solvent

This is the accepted version of this paper. Paper can be referenced as:
P. Christensen, Z. Milojevic, M.S. Wise, M. Ahmeid, P.S. Attidekou, W. Mrozik, N.A. Dickman, F. Restuccia, S.M.Lambert, P.K. Das. *Thermal and mechanical abuse of electric vehicle pouch cell modules*, Applied Thermal Engineering, 2021. https://doi.org/10.1016/j.applthermaleng.2021.116623

[3][33] which will condense on contact with cooler air: such a mixture could result in a vapour cloud explosion [34] if ignited in a confined space with the required concentration of oxygen. The explosion of the Surprise LiBESS has been reported[14][15] to have taken place when a pair of cells in a single module (28 64Ah NMC pouch cells arranged as 14 parallel pairs in series per module, 14 modules per vertical rack[14][15]) were forced into thermal runaway either by lithium dendrites penetrating the separator[14] or arc heating[15]. This produced a gaseous mixture which included H_2, C_2H_4, CH_4, CO, and CO_2[14] and which we believe also contained a range of small chain alkanes, HCN, HF, NOx and droplets of solvent [3][8][10][25][33] (and see discussion below), in other words a vapour cloud. The Novac 1230 fire suppressant which was released 30 s after the laser smoke detection system triggered displaced oxygen from the container and hence prevented ignition: the gasses continued to be produced as adjacent cells and modules went into thermal runaway, without any fire. When the fire department arrived on the scene, "low lying white clouds of gas/vapour mixture were observed issuing from the structure" [16]: see Figure 9(c) below. On opening the door of the container some 3 hours after the smoke alarm, it has been postulated [15] that the hot gases near the ceiling of the container billowed and touched a hot module, triggering the violent vapour cloud explosion.

As with experiment 1 above, swelling of the pouch cells was not observed in experiment 2: however, in contrast to experiment 1 above, flare-like flames were ejected from the front of the module, which was the strongest point of the casing.

Figure 7(a) shows plots of the thermocouple temperatures along with the temperature of the module at the point of impact obtained from the thermal images up to thermal runaway, and the voltage V_2 of the top quartet of cells, and Figures 7(b) and (c) show all the DAQ data for the experiment.

As may be expected, the responses of the thermocouples lag significantly behind that of the thermal camera, see Figure 7(a), as the data from the latter were taken from an area immediately adjacent to the point of impact, as can be seen in the inset to the figure. In addition, the temperature of the underside of the module increased more slowly than that of the module on the top face, again as may be expected.

This is the accepted version of this paper. Paper can be referenced as:
P. Christensen, Z. Milojevic, M.S. Wise, M. Ahmeid, P.S. Attidekou, W. Mrozik, N.A. Dickman, F. Restuccia, S.M.Lambert, P.K. Das. *Thermal and mechanical abuse of electric vehicle pouch cell modules*, Applied Thermal Engineering, 2021. https://doi.org/10.1016/j.applthermaleng.2021.116623

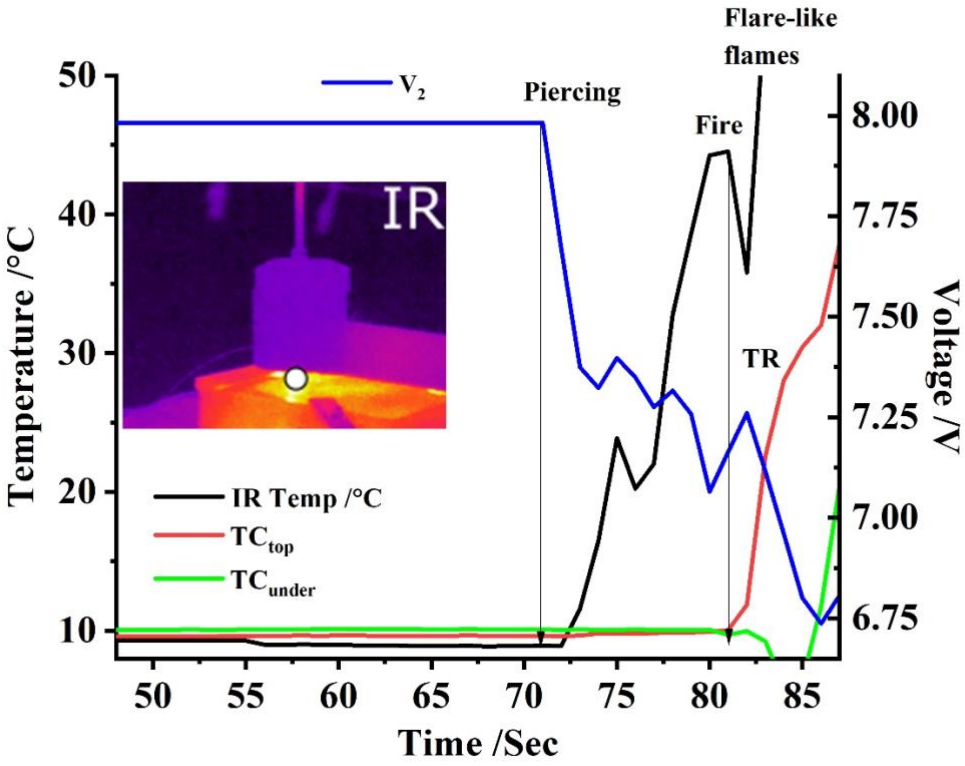

(a)

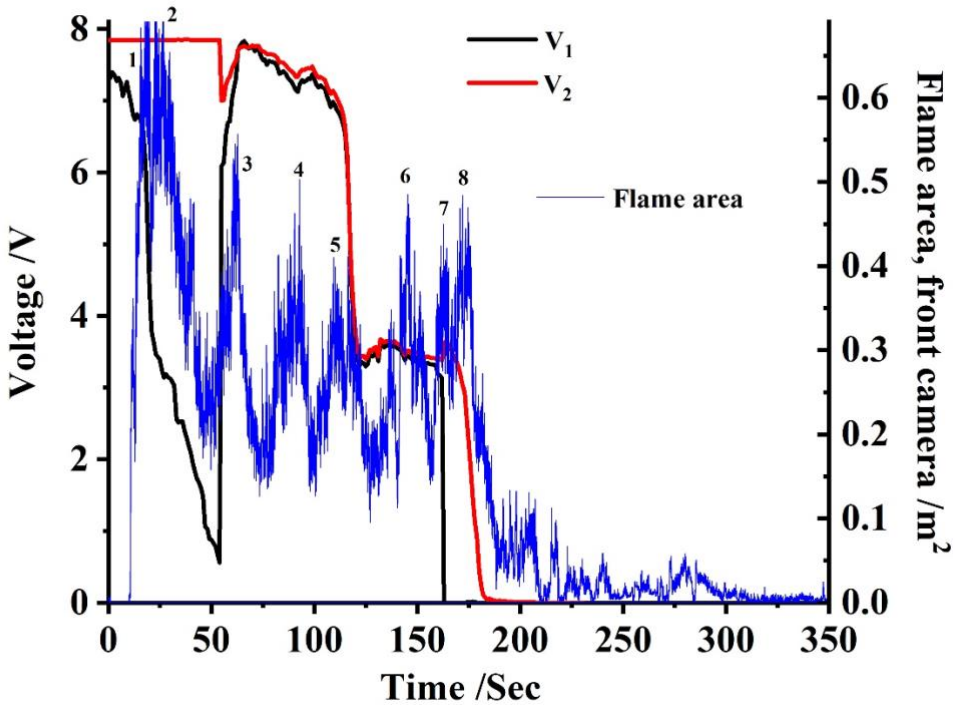

(b)

This is the accepted version of this paper. Paper can be referenced as:
P. Christensen, Z. Milojevic, M.S. Wise, M. Ahmeid, P.S. Attidekou, W. Mrozik, N.A. Dickman, F. Restuccia, S.M.Lambert, P.K. Das. *Thermal and mechanical abuse of electric vehicle pouch cell modules*, Applied Thermal Engineering, 2021. https://doi.org/10.1016/j.applthermaleng.2021.116623

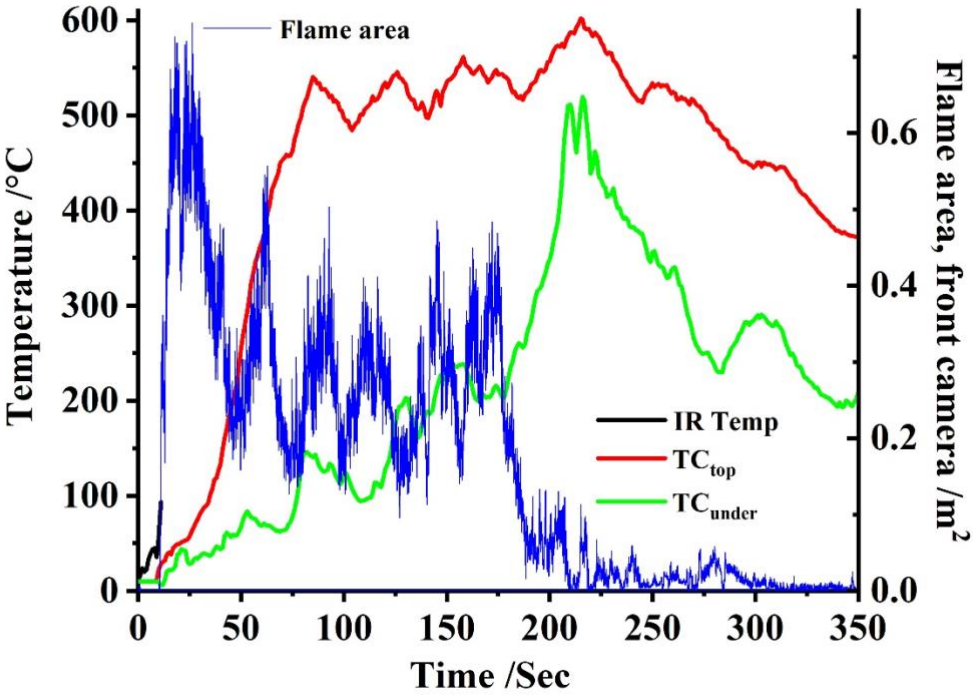

(c)

Figure 7. The DAQ and thermal imaging data collected during the nail piercing experiment 2 at the DNV GL site, and the flame areas calculated from the front optical camera. (a) Up to thermal runaway: (b) and (c) all data. (b) Flames areas, thermocouple and thermal imaging data and (c) cell voltage and flame areas.

The voltage of the top quartet of cells collapsed immediately, see Figure 7(b), and in a single step after penetration at ca. 50 V min^{-1} from 8V to ca. 0.6V as the temperature reached ca. 324 ˚C. However, and very surprisingly, the voltage then recovered to ca. 6.3V at 168 V min^{-1} before increasing more slowly to 7.8V before decreasing again as the temperature on the top face of the module reached 420 ˚C: this collapse was in two stages, again reflecting the sequential failure of the parallel pairs of cells. The first step tracked that of the lower quartet of cells, and occurred at ca. 50 V min^{-1}. The remaining two parallel cells of the top quartet then decreased faster (100 V min^{-1} c.f.f. 24 V min^{-1}) and 36 s earlier than the remaining parallel cells in the lower quartet. The varying thermocouple responses reflect the effect of the flames licking around them.

This is the accepted version of this paper. Paper can be referenced as:
P. Christensen, Z. Milojevic, M.S. Wise, M. Ahmeid, P.S. Attidekou, W. Mrozik, N.A. Dickman, F. Restuccia, S.M.Lambert, P.K. Das. *Thermal and mechanical abuse of electric vehicle pouch cell modules*, Applied Thermal Engineering, 2021. https://doi.org/10.1016/j.applthermaleng.2021.116623

Figures 7(b) and (c) show the flame areas calculated from the front video camera data (the rear camera failed to record): as can be seen, the ignition of the various cells is shown by the various flame area peaks, where the flame areas drop after the initial peaks from the ignition of a new cell, and then spike to a peak again when the next cell ignites. From the figures, it is clear that the magnitude of the maximum flame areas varied between ca. 0.4 - 0.7 m^2, at each cell ignition. As the last cell ignited, the flame area quickly reduced as the remaining flames were simply due to the remaining burning plastic.

In terms of the failure of individual cells, Figure 7(c) suggests that the cells fail as in the order shown in Figure S11.

Abaza et. al.[7] and Zhao and co-workers [35] postulate that a high rate of voltage collapse during nail penetration indicates a low short-circuit resistance, and that this determines the short circuit current and hence the heating rate and temperature rise. The short-circuit resistance R_s is given by:

$$R_s = R_{nail} + R_{cnt} \qquad (1)$$

where R_{nail} is the resistance of the nail and R_{cnt} the contact resistance. However, the variability across nominally identical experiments [7] suggests that this may be a somewhat over-simplistic model, and the data in Figure 7(c) definitely support this critique as, despite having all been penetrated, all eight cells are sustaining significant voltages some 2 minutes after thermal runaway was marked by the appearance of the flare-like flames and with temperature of the top surface of the module at over ca. 500 ˚C. Yokoshima and co-workers [36] have suggested a more sophisticated circuit model of nail penetration involving multiple cells. The authors employed X-Ray imaging to study the nail penetration of $LiCoO_2$ pouch cells in-situ: they observed increases in cell voltage after penetration as well as the melting of the nail and the boiling of the organic solvent of the electrolyte (ethylene carbonate, diethylene carbonate and lithium hexaflurorophosphate) due to the high short circuit current densities and consequent Joule heating. The increase in cell voltage was ascribed to the breaking of the internal short circuit through the nail due to the melting of the nail and the boiling away of the electrolyte. They also observed a white gas which they linked to the boiling electrolyte. Thus the initial collapse of the cell voltages of the top quartet of cells in Figure 7(c) must be due to the initial short circuiting of the four cells by the nail: the recovery logically must then be due to the loss of the short circuit, which may be due to the boiling away of the electrolyte

This is the accepted version of this paper. Paper can be referenced as:
P. Christensen, Z. Milojevic, M.S. Wise, M. Ahmeid, P.S. Attidekou, W. Mrozik, N.A. Dickman, F. Restuccia, S.M.Lambert, P.K. Das. *Thermal and mechanical abuse of electric vehicle pouch cell modules*, Applied Thermal Engineering, 2021. https://doi.org/10.1016/j.applthermaleng.2021.116623

around the nail and/or melting of the aluminium current collectors: given that the melting points of aluminium and copper are 660 ˚C and 1083 ˚C, respectively, it is most likely the former that melts away from the nail and breaks the circuit. Recent studies by Feng and co-workers [37][38] provide a complementary explanation of the data in Figure 7(c), involving the vaporisation of the electrolyte and this is covered in the Discussion section below.

Again, the data in Figure 7(c) strongly suggest that, at least for this chemistry and form factor, voltage drop cannot be employed as an early warning of thermal runaway.

Abaza and co-workers [7] investigated the nail penetration of 15 Ah NMC+LMO pouch cells and stated that such abuse should not result in the swelling of the cells as the gases produce could escape past the nail: however, they did observe swelling. Two further nail penetration experiments were carried out at the DNV GL site, differing from experiment 2 only in the location of the penetration (middle of the casing and in the lower corner, see Figure S8), and in both cases, the cells swelled before popping and ejecting dense white vapour before the vapour ignited. In experiment 3, the cells expanded for 6 s after nail penetration before popping after which they ejected dense white vapour for 2 s which then ignited. In experiment 4, the cells expanded for 4 s before popping, ejecting both thick black smoke and white vapour, igniting 10 s after a significantly audible popping: black smoke has been attributed to the ejection of cathode particles[37][39]. Flare-like flames were seen in both experiments, emerging from the rear and side of the module in both cases, in contrast to experiment 2. In both cases, the cell voltages of the top quartet of cells collapsed in a single step after which the voltage of the lower quartet collapsed, 96 s and 48 s for experiments 3 and 4, respectively, after nail penetration as was observed in experiment 2.

3.2.2 Fire Services College experiments 1 & 2

The first experiment at the Fire Services College was a nail penetration between the tabs, identical to experiment 2 at the DNV GL site except the module was charged to c. a. 4.03V, i.e. 75% SOC. The same sequence of events were observed as in the DNV GL experiment, see Figures 8(a) – (f): a wisp of white vapour as soon as the nail penetrated 0.532 s (a) and 0.538 s (b), then the evolution of thick white vapour followed by (in this case) the almost immediate ignition of the vapour 3.794 s (c) and 3.858 s (d), then flare-like flames from the front, side and rear of the module (e) 100.567 s (e) and 82.6 s (f) after penetration.

This is the accepted version of this paper. Paper can be referenced as:
P. Christensen, Z. Milojevic, M.S. Wise, M. Ahmeid, P.S. Attidekou, W. Mrozik, N.A. Dickman, F. Restuccia, S.M.Lambert, P.K. Das. *Thermal and mechanical abuse of electric vehicle pouch cell modules*, Applied Thermal Engineering, 2021. https://doi.org/10.1016/j.applthermaleng.2021.116623

Following on from the previous experiment, and experiment 2 at the DNV GL site, the aim of experiment 2 at the FSC was to assess the validity the generally-held perception that higher SOC's represent more of a hazard [3][40], particularly in terms of toxic and flammable gas release [25], and involved a repeat of the 75% SOC experiment at 50% SOC.

Figures 9(a) – (c) show stills from the video taken of the experiment: (a) was 26.47 s after the nail penetrated the module; (b) was 35.47 s after penetration and (c) 52.13 s after. The white vapour did not ignite during the experiment and, as can be seen from the figure, was clearly heavier than air, rolling across the ground, pushed by the slight breeze running from right to left in the images.

(a)

(b)

(c)

(d)

This is the accepted version of this paper. Paper can be referenced as:
P. Christensen, Z. Milojevic, M.S. Wise, M. Ahmeid, P.S. Attidekou, W. Mrozik, N.A. Dickman, F. Restuccia, S.M.Lambert, P.K. Das. *Thermal and mechanical abuse of electric vehicle pouch cell modules*, Applied Thermal Engineering, 2021. https://doi.org/10.1016/j.applthermaleng.2021.116623

(e) *(f)*

Figure 8. Images taken during experiment 1 at the FSC (nail penetration at 75% SOC): (a) 0.532s, (b) 0.538s, (c) 3.794s, (d) 3.858s, (e) 10.567s and (f) 82.6s after nail penetration.

(a) *(b)*

(c)

Figure 9. Stills from the video taken of experiment 2 at the Fire Services College: nail penetration at 50% SOC. Image (a) was taken 26.47 s after the nail penetrated the module completely; (b) was 35.47 s after penetration and (c) 52.13 s after penetration.

This is the accepted version of this paper. Paper can be referenced as:
P. Christensen, Z. Milojevic, M.S. Wise, M. Ahmeid, P.S. Attidekou, W. Mrozik, N.A. Dickman, F. Restuccia, S.M.Lambert, P.K. Das. *Thermal and mechanical abuse of electric vehicle pouch cell modules*, Applied Thermal Engineering, 2021. https://doi.org/10.1016/j.applthermaleng.2021.116623

Figures 10(a) - (d) show plots of the gas sensor, thermocouple and thermal readings taken during the experiment.

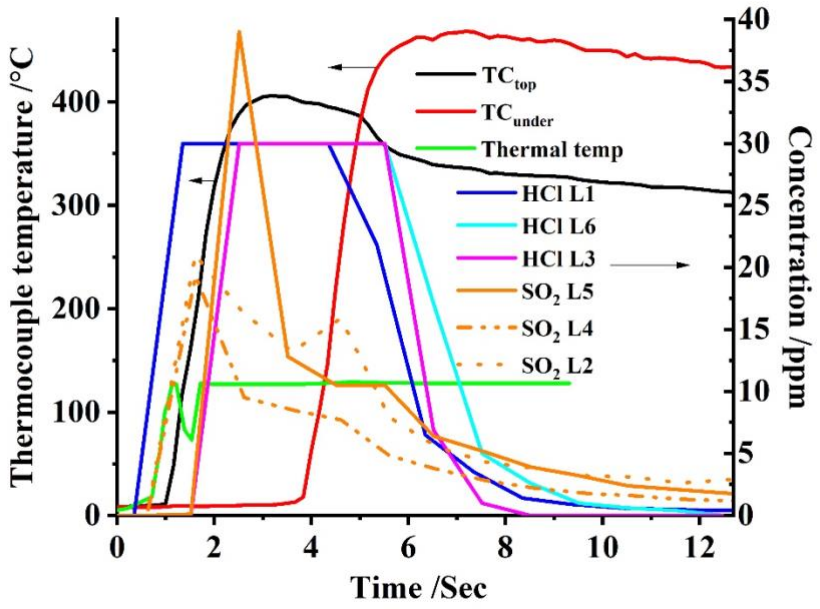

(a)

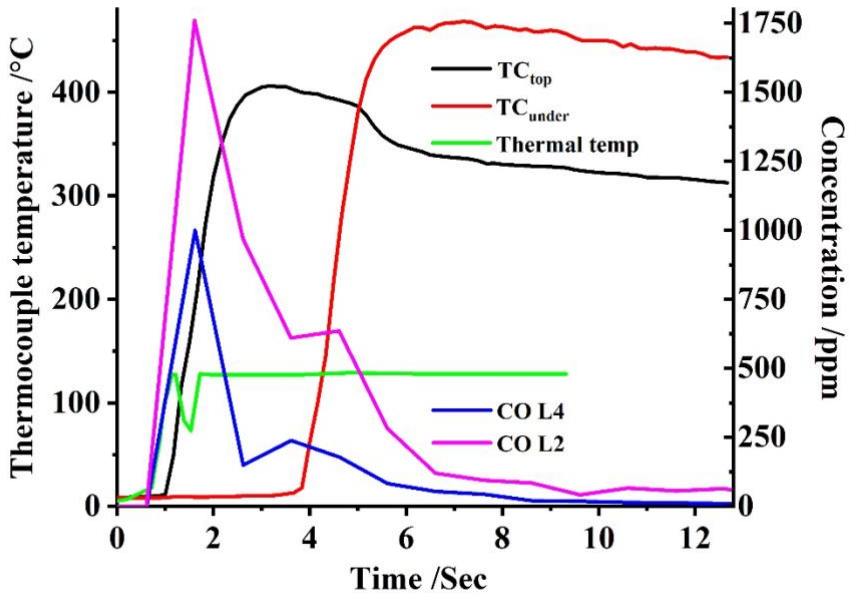

This is the accepted version of this paper. Paper can be referenced as:
P. Christensen, Z. Milojevic, M.S. Wise, M. Ahmeid, P.S. Attidekou, W. Mrozik, N.A. Dickman, F. Restuccia, S.M.Lambert, P.K. Das. *Thermal and mechanical abuse of electric vehicle pouch cell modules*, Applied Thermal Engineering, 2021. https://doi.org/10.1016/j.applthermaleng.2021.116623

(b)

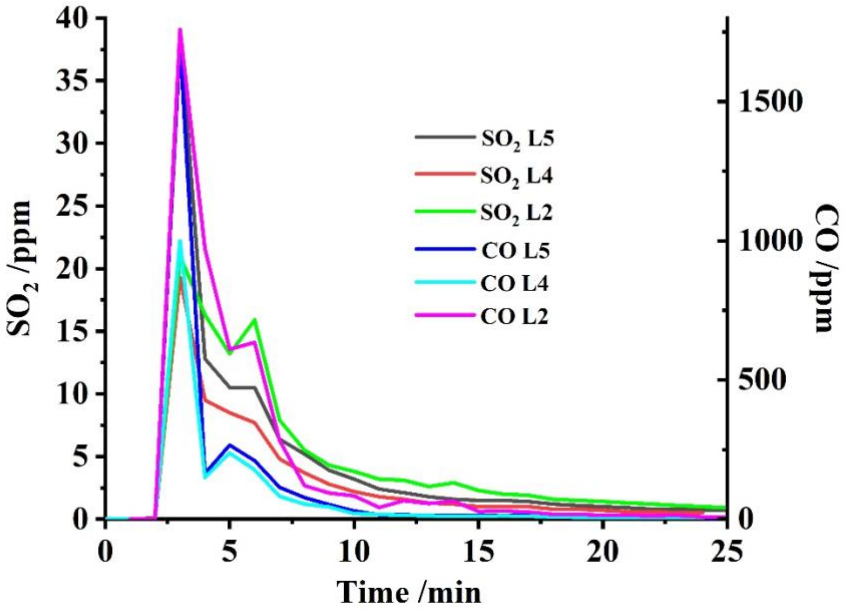

(c)

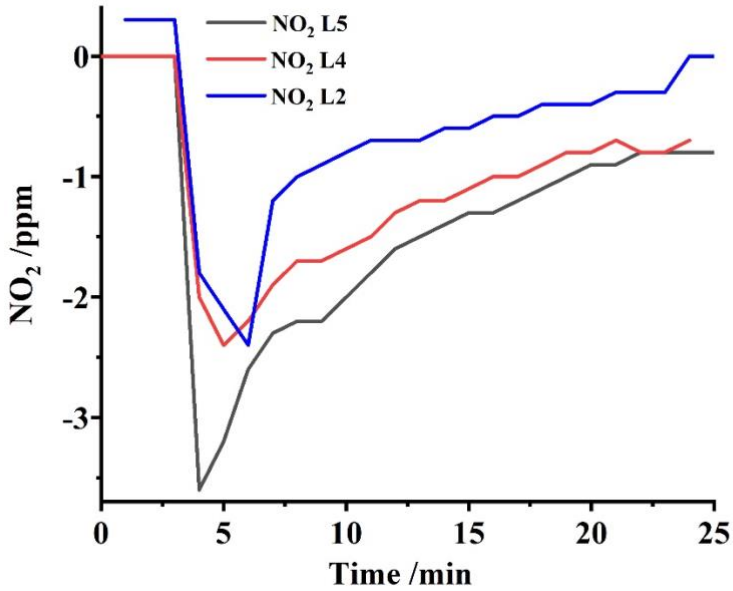

(d)

This is the accepted version of this paper. Paper can be referenced as:
P. Christensen, Z. Milojevic, M.S. Wise, M. Ahmeid, P.S. Attidekou, W. Mrozik, N.A. Dickman, F. Restuccia, S.M.Lambert, P.K. Das. *Thermal and mechanical abuse of electric vehicle pouch cell modules*, Applied Thermal Engineering, 2021. https://doi.org/10.1016/j.applthermaleng.2021.116623

Figure 10. (a) and (b) plots of the concentrations of the various gases detected during experiment 2 at the Fire Services College and the thermocouple and thermal camera temperatures, (a) CO and (b) HCl/HF and SO_2. Concentrations of (c) CO & SO_2 and (d) NO_2/HCN* observed during the experiment. * See text for details.*

As can be seen from Figure 10(b), the HCl/HF sensors went over their maximum range of 30 ppm: the locations L1 – L6 correspond to those on Figure S7.

Table 5 summarizes the maximum sensor readings observed during the experiment and the times that they occurred after nail penetration.

Gas	**Location**	**Time /Min**	**Max. conc. /ppm**	**Comments**
CO	2	3	1760	
	4	3	1000	
	5	3	1710	
SO_2	2	3	21	
	4	3	19.3	
	5	3	39	
NO_2	2	6	-2.4	Interference by HCN
	4	5	-2.4	
	5	4	-3.6	
HCl	1	1 - 5	30	Over range
	3	2 - 6	30	Over range
	6	2 - 6	30	Over range

Table 5. Summary of the maximum gas sensor readings observed during experiment 2 at the Fire Services College.

During thermal runaway of LiBs and prior to ignition, a variety of gases are produced within the cells and vented to the atmosphere, including HF, CO_2, CO, H_2, a wide range of small chain alkanes and alkenes [3][8][10][25][33][41] and the solvents comprising the electrolyte such as ethylene carbonate and dimethyl carbonate [3][33]. The response of the NO_2 sensor suggests that HCN was also produced, and this compound has been reported previously [40][42][43][44], and, as was stated above, the personal protective equipment of the first responders attending the explosion of the LiBESS at Surprise were contaminated with HCN [17].

This is the accepted version of this paper. Paper can be referenced as:
P. Christensen, Z. Milojevic, M.S. Wise, M. Ahmeid, P.S. Attidekou, W. Mrozik, N.A. Dickman, F. Restuccia, S.M.Lambert, P.K. Das. *Thermal and mechanical abuse of electric vehicle pouch cell modules*, Applied Thermal Engineering, 2021. https://doi.org/10.1016/j.applthermaleng.2021.116623

The data in the table suggest that the heavier-than-air SO_2 filled the lower part of the container and drifted with the wind past the door. Interestingly, the time dependence of its concentration matched exactly that of CO, see Figure 10(d), and all sensors showed the CO and SO_2 reaching their maximum concentrations 3 minutes after nail penetration. This was confirmed during the other two experiments at the College (nail penetration at 75% SOC and overcharge of two of the cells in one of the modules of a 5-module stack), suggesting the two gases had a common origin. Reductive additives to aid SEI formation typically contain sulphur [45] including SO_2, CS_2, polysulfide, cyclic alkyl sulfites such as ethylene sulfite and propylene sulfite, and aryl sulfites. Sulphur may also come from alternative lithium salts such as LiFSI [46]. However, ethylene sulphite is commonly employed in LiBs [47][48][49][50] and hence it is highly likely that this additive is the source of the SO_2 and at least some of the CO.

The amount of vapour released within the container, unlike the other experiments where the vapour ignited almost immediately after release, allowed a much larger area of the container to be saturated by a flammable mixture. If this mixture were to ignite, there could be a possibility of a flash fire, fire balls developing, or in extreme cases even a vapour cloud explosion. The severity of the deflagration event would depend on the amount of overpressure generated as the flame accelerates at significant speed in the vapour cloud. Any of these scenarios would be extremely dangerous [51].

Figure 11 shows plots of the thermocouple temperatures and cell voltages observed during the experiment. In contrast to the experiments where the vapour ignited causing the thermocouple readings to fluctuate due to the flames, the first derivatives of the thermocouple readings from experiment 2 at the College showed a homologous response, see Figure S12 with a single, well-defined maximum for each thermocouple.

This is the accepted version of this paper. Paper can be referenced as:
P. Christensen, Z. Milojevic, M.S. Wise, M. Ahmeid, P.S. Attidekou, W. Mrozik, N.A. Dickman, F. Restuccia, S.M.Lambert, P.K. Das. *Thermal and mechanical abuse of electric vehicle pouch cell modules*, Applied Thermal Engineering, 2021. https://doi.org/10.1016/j.applthermaleng.2021.116623

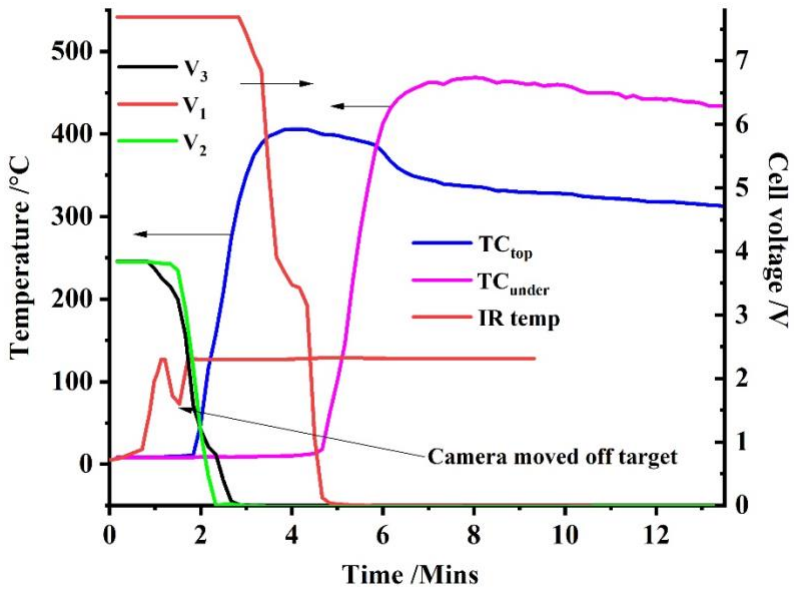

Figure 11. The DAQ data collected during the nail piercing experiment 2 at the FSC site and the temperature recorded by the thermal camera.

As can be seen from the figure, despite the fact that the nail penetrated all the cells, whilst the voltages of the top four cells collapsed fairly soon after penetration, the lower four cells retained their charge for ca. 2 minutes.

Figures S13(a) and (b) show stills taken from the thermal camera video 60 s and 143 s, respectively, after nail penetration. Throughout the experiment, solid objects were ejected from the module and bounced as they hit the ground; these objects appeared to be at temperatures ≤ ca. 100 ˚C, i. e. showing white in (a), circled. These events were not visible to the naked eye and did not appear in the optical video due to the dense vapour. Also clearly visible in (a) is a jet of vapour being ejected horizontally. In Figure S13(b), liquid can be seen dropping from the module (circled), which also registered as ≤ ca. 100 ˚C. The temperature in the target sights did not rise above ca. 129 ˚C throughout the experiment.

4.0 Discussion

As the DNV GL experiments were conducted in an entirely open environment, and the FSC experiments were in the partially contained environment of an open container, the boundary conditions constraining the escaping gases and the local environmental temperature during the battery fires were highly likely to be

This is the accepted version of this paper. Paper can be referenced as:
P. Christensen, Z. Milojevic, M.S. Wise, M. Ahmeid, P.S. Attidekou, W. Mrozik, N.A. Dickman, F. Restuccia, S.M.Lambert, P.K. Das. *Thermal and mechanical abuse of electric vehicle pouch cell modules*, Applied Thermal Engineering, 2021. https://doi.org/10.1016/j.applthermaleng.2021.116623

different, hence affecting the flame lengths. The maximum vertical and horizontal flame lengths measured via image processing in each experiment are show in Figure 12. Experiments 2, 3 and 4, all nail penetration experiments but with penetration at different points on the modules, showed different maximum flame lengths, with a maximum flare of 217 cm observed.

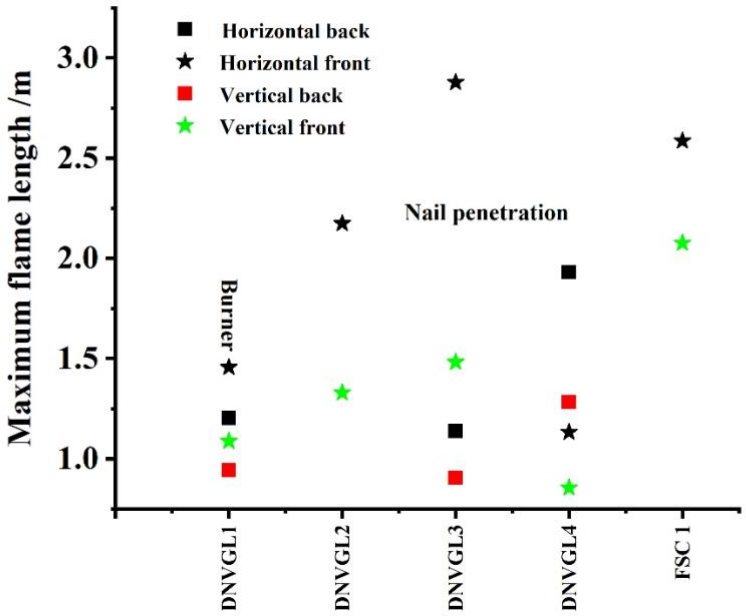

Figure 12. Maximum vertical and horizontal flame lengths measured in DNV GLS experiments 1 - 4 and FSC experiment 1.

It can be seen from Figure 12 that the maximum flare length was observed in experiment 1 at the FSC (75% SOC, nail penetration). The maximum flame length measured was 275 cm, which is ca. 9 times the length of the module itself. Hence, careful consideration must be made in safety designs to account for safety distance, as from these observations any flammable material or mixture up to 275 cm from the pack could receive intense and rapid heating rates from these flares in the case of a module failure.

It is worth noting that there are few studies reporting SO_2 and hence, ideally, the mechanism by which this is produced requires further attention. In our case, the yield of SO_2 was significantly higher in the 50% SOC experiment (19 – 39 ppm) than in the 75% SOC test (5.1 ppm – data not shown). This is in agreement with the work of Lecocq et al. [46], who found that more SO_2 was released at lower SOCs, but contrary to other studies [25][40][52] reporting higher amounts of SO_2 at the higher SOCs (albeit for different chemistries).

This is the accepted version of this paper. Paper can be referenced as:
P. Christensen, Z. Milojevic, M.S. Wise, M. Ahmeid, P.S. Attidekou, W. Mrozik, N.A. Dickman, F. Restuccia, S.M.Lambert, P.K. Das. *Thermal and mechanical abuse of electric vehicle pouch cell modules*, Applied Thermal Engineering, 2021. https://doi.org/10.1016/j.applthermaleng.2021.116623

Carbon monoxide has been identified as one of the main constituents of the gas released during thermal runaway [52][53][54][55][56]. Ribiere et al. [40] found that the amount of CO produced increased with SOC, and this has been confirmed by other studies [25][42][57]. However, it appears the cathode chemistry of the LiB has a major influence on the gases produced: thus Said et al. [58] found comparable levels of CO for LCO and NMC, but an order of magnitude less for LFP; Golubkov et al. [59] found much higher amounts of CO released from LFP compared to NCA. Sun et. al. [25] found that the amount of CO released was in the order: LMO>LFP>LCO> NMC, with LMO producing almost as twice as much CO as NMC. The authors concluded that a 10Ah pouch cell could produce more than 10,000 ppm CO, which exceed levels that that can cause serious sickness, and even death (1000–2000 ppm in 1–2 min). During our experiments, the CO reached concentrations of 1000-1760 ppm in 3 minutes. This suggest a potentially serious threat to health and life just from this component of the white vapour. Ribière and coworkers [40] have evaluated the toxicity levels of the fumes from burning LiBs, based on their work on LMO cells which has allowed the estimation of the battery energy in Wh that could lead to exposure above the Immediate Effects Threshold (IET) and the First Lethal Effects Threshold (FLET) caused by 60 mins exposure to a LiB fire in a 50 m^3 room, and typical data are shown in Table 6. Thus a single burning 236 Wh pouch cell in a 50 m^3 unventilated room would take 2.8 minutes and 5.1 minutes to reach the IET and FLET of HF, respectively. The same times would be required for a burning 8 cell, 53.8 Ah module in a 400 m^3 room.

/Wh	HF	CO	NO	SO_2	HCl
IET	60	290	280	530	1320
FLET	110	1140	2080	4710	7880

Table 6. Immediate effects thresholds and first lethal effects thresholds for various gases produced by lithium ion cells during the thermal runaway[37].

The thermal runaway of LiBs has been studied in depth of late [3][37][38][60][61], and the steps involved in thermal runaway are broadly accepted as[3]:

1. The breakdown of the Solid Electrolyte Interface (SEI). The Solid Electrolyte Interface (SEI) is the other front-line safety system: LIBs are unique in battery technology in that the fully-lithiated graphite anodes typically employed have ca. the same redox potential as that of metallic lithium [62] and hence should immediately reduce the organic carbonates employed in the electrolyte to hydrogen, various flammable gaseous hydrocarbons and heat [63]. The reason that this does not occur is the serendipitous formation of a protective barrier, the SEI, which is permeable to lithium

This is the accepted version of this paper. Paper can be referenced as:
P. Christensen, Z. Milojevic, M.S. Wise, M. Ahmeid, P.S. Attidekou, W. Mrozik, N.A. Dickman, F. Restuccia, S.M.Lambert, P.K. Das. *Thermal and mechanical abuse of electric vehicle pouch cell modules*, Applied Thermal Engineering, 2021. https://doi.org/10.1016/j.applthermaleng.2021.116623

ions, between the anode and solvent during the first charge. The SEI continuously varies in thickness during the life of the battery, but overall increasing in thickness and incorporating lithium ions as it does so [64]. The exact composition of the SEI is unknown, although it is known to incorporate lithium ions and is likely be dynamic: it is generally represented as lithium salts of carbonate fragments, and the breakdown of the SEI may be represented as [3]:

$$(CH_2OCO_2Li)_2 \rightarrow Li_2CO_3 + C_2H_4 + CO_2 + 1/2\ O_2 + \text{heat} \quad (3)$$

This commences around 60 – 70 ˚C, but the SEI is able to self-heal up to 80 – 120 ˚C [22][38], albeit to form a less-effective barrier to the solvent. Feng and co-workers [22] suggest that there are three stages: (1) initial SEI decomposition 80 – 120 ˚C; (2) the balanced region between 120 and 250 ˚C where the self-healing rate is equal to the rate of decomposition and (3) thermal runaway above 250 ˚C due to separator collapse, major internal short circuit and hence rapid increase in temperature. Wang et. al. [65] have reported that the activation energy barrier for the decomposition of the SEI, and the onset temperature, both decrease with increasing SOC.

2. The reduction of the organic carbonate solvent by exposed lithiated graphite. Once holes form in the SEI, direct reduction of the solvent can take place which can be represented in general terms as:

$$2Li + C_xH_yO_z \rightarrow Li_2CO_3 + C_{x-1}H_4 + \text{heat} \quad (4)$$

Where [3] $C_xH_yO_z$ is an organic carbonate (e.g. $C_3H_4O_3$, ethylene carbonate EC; $C_3H_6O_3$, dimethyl carbonate DMC; $C_4H_8O_3$ ethyl methyl carbonate EMC, $C_5H_{10}O_3$ diethyl carbonate DEC and $C_4H_6O_3$ propylene carbonate PC), $C_{x-1}H_4$ represents a number of short chain alkanes and alkenes and Li represents the lithium in the graphite. CO is also generated by reaction with the solvent, e.g.:

$$C_3H_6O_3 + 2Li \rightarrow 2CH_3OLi + CO \quad (5)$$

Hydrogen is produced via reduction of the binders employed in the cells (e.g. PVDF[3]). This becomes significant at temperatures where the SEI does not self-heal.

This is the accepted version of this paper. Paper can be referenced as:
P. Christensen, Z. Milojevic, M.S. Wise, M. Ahmeid, P.S. Attidekou, W. Mrozik, N.A. Dickman, F. Restuccia, S.M.Lambert, P.K. Das. *Thermal and mechanical abuse of electric vehicle pouch cell modules*, Applied Thermal Engineering, 2021. https://doi.org/10.1016/j.applthermaleng.2021.116623

3. Melting and collapse of the separator. The temperature at which collapse of the separator is initiated depends upon composition: e.g. the melting point of polyethylene is 130 ˚C, polypropylene 170 ˚C and ceramic-coated polymer/mixed polymer separators ca. 200 ˚C [3][22]. However, melting may not result in the immediate collapse of the separator structure. Once the integrity of the separator is lost, significant internal short circuits can occur and, until the work of Feng and co-workers [37][38][66], this was considered to be the trigger and main driving force behind thermal runaway [2][22][32].
4. The exothermic collapse of the cathode structure to generate oxygen as well as (in certain cases) highly oxidising oxides [22]: the onset temperature at which this occurs is highly dependent upon the oxide, e.g. from 150 ˚C to 310 ˚C [3][22]. The oxygen then exothermically oxidizes the organic solvents in the electrolyte [55].

The mechanism of thermal runaway following overcharge involves the same steps as discussed above, but is initiated by the over-lithiation of the anode to form lithium metal at the surface [67] and the exothermic delithiation and collapse of the cathode structure [3] resulting in increased resistance and hence Joule heating. The lithium metal will exothermically reduce the solvent as detailed above, and can form dendrites which grow through the separator to cause an internal short circuit. When the temperature exceeds that of the melting point of lithium, 180 ˚C [68] this will also result in an internal short circuit. Lithium plating is increased with increasing temperature [69] suggesting that cells retaining their charge but under thermal abuse from adjacent cells could show enhanced lithium plating.

The model discussed above has become increasingly challenged: thus there remains no clear and quantitative definition of thermal runaway[32][37], there is disagreement as to whether gases are vented before or during thermal runaway from prismatic or cylindrical cells and the exact nature of the gases produced[33][37][39]. In addition, there are new theories of thermal runaway and refinements of the current, rather generalised "model". Thus, Liu and co-workers[70] have shown that the oxygen produced as the cathode structure collapses is consumed at the anode ("chemical crosstalk") in a highly exothermic process (ca. 7x more heat produced than from cathode collapse alone) which can commence at 150ºC (e.g. for NMC cathodes), significantly below the temperature for the collapse of the more stable separators (e.g. PET nanofibers, 257 ˚C) and hence thermal runaway can be initiated without the need for separator collapse and concomitant significant ISC. There is also increasing evidence that thermal runaway may not simply be defined as a temperature rise of 1ºC s^{-1} if thermal runaway is more generally defined as a self-sustaining

This is the accepted version of this paper. Paper can be referenced as:
P. Christensen, Z. Milojevic, M.S. Wise, M. Ahmeid, P.S. Attidekou, W. Mrozik, N.A. Dickman, F. Restuccia, S.M.Lambert, P.K. Das. *Thermal and mechanical abuse of electric vehicle pouch cell modules*, Applied Thermal Engineering, 2021. https://doi.org/10.1016/j.applthermaleng.2021.116623

heating process, i.e. once the temperature of a cell passes a point of no return, the exothermic reactions continue to generate heat and the cell will progress inevitably to an exponential increase in temperature[71]. It has been stated that[33] if the electrolyte boils away from a cell, thermal runaway cannot happen: a simple search of the literature proves this is not the case, with venting of electrolyte succeeded by thermal runaway[71]. Moreover, recently, Feng and co-workers [37][38] have shown that lithiated graphite anode and NMC cathode powders can undergo a direct and highly exothermic solid state redox reaction at temperatures ≥ ca. 250 ˚C (presumable the via the transfer of lithium ions) and have proposed that internal short circuit initiates thermal runaway but is not responsible for its propagation. Instead, the internal short circuit generates sufficient Joule heating for significant vaporisation of the solvent to take place this, coupled with the collapse of the separator allows direct electrochemical reaction between anode and cathode which generates sufficient heat to raise the temperature above 800 ˚C and perpetuate thermal runaway.

Temperature is often quoted as a potential early signal of thermal runaway: however, overcharging can result in little or no temperature change; i.e. a few degrees during the overcharge process[71], whilst there can be a wide variation in temperature across the can of a lithium ion cell subjected to thermal abuse[33].

There is a major dearth of system-level research as opposed to cell- or module- level: such studies are becoming increasingly critical as it is becoming apparent that self-ignition may occur at lower temperatures in larger assemblies of cells/modules[64].

Finally, the composition, ubiquitous nature and hazards of the white vapour have not been recognised. In our view, the white vapour is produced by the pyrolysis of the electrolyte by the heat generated in thermal runaway. This gas cannot ignite within the cells as the oxygen produced during thermal runaway is insufficient to sustain combustion[3], which thus takes place once the gases produced exit the cell and if there is an ignition source present or via friction between gas and the exit point, and the cell SOC is > 50%. The latter point is interesting as, for example at 50% SOC, there should still be a sufficient stored electrical energy for arcing to occur and provide an ignition source. Feng et. al.[37] suggest that the “white smoke” is primarily due to solvent vaporised prior to thermal runaway, and that such venting happens at successively higher temperatures as the various components vaporise. We disagree with two key facts: venting from the pouch cells studied by us takes place during thermal runaway, and the white vapour not only contains condensed solvent droplets but also pyrolysis products, as can be seen from the gas sensor data obtained during the experiments at the FSC: further, evidence for pyrolysis comes from the observation of the tied

This is the accepted version of this paper. Paper can be referenced as:
P. Christensen, Z. Milojevic, M.S. Wise, M. Ahmeid, P.S. Attidekou, W. Mrozik, N.A. Dickman, F. Restuccia, S.M.Lambert, P.K. Das. *Thermal and mechanical abuse of electric vehicle pouch cell modules*, Applied Thermal Engineering, 2021. https://doi.org/10.1016/j.applthermaleng.2021.116623

evolution of SO_2 and CO. The black smoke observed in DNV GL experiment 4 may be attributed to the melting of the aluminium current collectors and concomitant ejection of the cathode active material[35]: this experiment of all the nail penetration tests was the only one where the thermocouple temperatures were comparable to the melting point of aluminium (600 ˚C[40]). White hot metal was ejected from both the overcharge experiments at the DNV GL site, suggesting molten aluminium, although Feng and co-workers have reported the melting of copper (m.p. 1083 ˚C[40]) during abuse experiments employing LCO cells[37].

Our data from experiment 2 at the DNV GL site supports the solid-state short circuit theory postulated by Feng et. al.[37][38][61]: from Figures 7(b) & (c) it can be seen that the revival of the cell voltage V_1 occurs when the temperature of the top of the module reaches 280 ˚C. The recent paper by He and co-workers [71] also supports the solid-state short circuit theory: the authors reported that the voltages of the cylindrical LCO cells employed in their experiments (1880 mAh) suddenly decreased during heating but, once all the electrolyte had been lost from the cells, the voltages were re-established. The authors made no comment on the phenomenon but it is clear that the behaviour is the same as that observed in our experiment 2 at the DNV GL site. Thus, in our experiment, the initial nail penetration and attendant Joule heating causes the voltage of only four of the cells in the module to collapse, despite all eight having been penetrated. Presumably, the short circuit between the other four is removed due to the aluminium current collectors melting away from the nail (as observed by Yokoshima et. al. [36]) with attendant vaporisation of the solvent around the nail. This then also happens with the remaining four cells, such that their voltage increases. The latter occurs during the production of flare-like flames as two of the cells fail, see Figure 7(c): the internal short circuit generates sufficient Joule heat to vaporize the solvent (producing white vapour, as observed in-situ by SEM [34], which ignites some seconds after exiting the cell) and cause the collapse of the separator. The latter is followed at temperatures greater than ca. 250 ˚C by direct contact of the (essentially dry) anodes and cathodes and a solid state redox reaction in which lithium ions are injected into the cathode and, perhaps, oxygen abstracted to form Li_2O, the reaction resulting in the production of significant amounts of heat and the thermal runaway and collapse of the remaining cells. The temperature of the top face of the module was ca. 250 ˚C at the start of the recovery of the cell voltage, see Figures 7(b) and (c).

5.0 Conclusions

The experiments in this paper were focused on the extremely important phenomenon of thermal process in runaway in lithium ion batteries, a key consideration with respect to the safe operation of these devices. In

This is the accepted version of this paper. Paper can be referenced as:
P. Christensen, Z. Milojevic, M.S. Wise, M. Ahmeid, P.S. Attidekou, W. Mrozik, N.A. Dickman, F. Restuccia, S.M.Lambert, P.K. Das. *Thermal and mechanical abuse of electric vehicle pouch cell modules*, Applied Thermal Engineering, 2021. https://doi.org/10.1016/j.applthermaleng.2021.116623

the experiments carried out in this paper, the behaviour of cells in thermal runaway was shown to depend strongly upon factors such as the nature of the abuse and the SOC.

The first visible indication of thermal runaway is the evolution of a thick, white vapour via the pyrolysis of the electrolyte: we believe that this is common across LiB cathode chemistries, form factors and manufacturers. This vapour is comprised of: H_2, SO_2, NO_2, HF, HCl, CO, CO_2, droplets of organic solvent and a large range of small chain alkanes and alkenes. If sufficient air is present, at high SOCs, > 50%, this vapour inevitably ignites in less than 1 minute. However, at low SOCs, ≤ 50%, the vapour may not ignite: and it will not ignite if insufficient air is present. As a result, in a confined space, there could be the possibility of a flash fire, fire balls developing, or in extreme cases, even a vapour cloud explosion. This explosion hazard, along with the toxicity of the white vapour, could be faced by first responders wherever large lithium ion batteries are present in an enclosed space and one or more cells are in thermal runaway. Thus as well as EV road traffic and LiBESS incidents, this includes incidents in storage warehouses, battery manufacturing plants, electric vehicle assembly plants, road, rail and sea transportation of EVs/battery packs, hybrid electric ships and ferries etc. As an additional problem, the white vapour could be mistaken for steam, especially following the extinguishing of fire.

Maximum flame flare lengths during the failure of the modules also reached up to 275cm, which highlights that any flammable material or mixture up to 275 cm from the pack could receive intense and rapid heating rates in the case of a module failure, something that needs to be considered for safety distance design.

Throughout these abuse experiments, the voltages of cells in modules engulfed in flames were maintained for many minutes: in addition, cell voltages have been observed to collapse during abuse, but then re-establish, negating their use as an early warning of thermal runaway. This finding is first analysed in this paper, and the latter phenomenon supports a wholly novel and recent theory in which thermal runaway is perpetuated following solvent venting via direct, solid-state electrochemical reaction between anode and cathode: this theory could have significant implications with respect to the design of safe, all-solid state lithium batteries.

6.0 Acknowledgements

This work was supported by the UK's Engineering and Physical Sciences Research Council (EPSRC) and the Faraday Institution (EP/S003053/1) as part of its Recycling of Li-Ion Batteries (ReLiB) project (FIRG005). The funders had no role in the study design, or the collation, analysis and interpretation of the

This is the accepted version of this paper. Paper can be referenced as:
P. Christensen, Z. Milojevic, M.S. Wise, M. Ahmeid, P.S. Attidekou, W. Mrozik, N.A. Dickman, F. Restuccia, S.M.Lambert, P.K. Das. *Thermal and mechanical abuse of electric vehicle pouch cell modules*, Applied Thermal Engineering, 2021. https://doi.org/10.1016/j.applthermaleng.2021.116623

data or the writing of this paper. The authors would like to thank Envision-AESC for the company's wholehearted support of the project, Newcastle University for a travel grant and Prof Guillermo Rein & Mr. Xuanze He for valuable discussions on experimental design.

References

1. Casey Grant, Executive Director of the US National Fire Protection Agency, private communication 14 October 2019, concerning the explosion at the Surprise Battery Energy Storage System.
2. P. Sun, X.Huang, R.Bisschop and H. Niu, Fire Technol., 56 (2020) 1361 – 1410.
3. Q. Wang, B. Mao, S. I. Stoliarov and J. Sun, Progress Energy Comb. Sci., 73 (2019) 95 – 131.
4. https://maritime.dot.gov/sites/marad.dot.gov/files/docs/innovation/meta/9616/hybrid-battery-refit-final-report-pics.pdf.
5. https://gcaptain.com/fire-and-gas-explosion-in-battery-room-of-norwegian-ferry-prompts-lithium-ion-power-warning/.
6. L. B. Diaz, X. He, Z. Hu, F. Restuccia, M. Marinescu, J. V. Barreras, Y. Patel, G. Offer and G. Rein, J. Electrochem. Soc., 167 (2020) 090559.
7. A. Abaza, S. Ferrari, H. K.Wong, C. Lyness, A. Moore, J.Weaving, M. Blanco-Martin, R. Dashwood, and R. Bhagata. J.Energy Storage, 16 (2018) 211 – 217.
8. D. Sturk, L. Hoffmann and A. Ahlberg Tidblad, Traffic Injury Prevention, 16 (2015) S159 - S164.
9. F. Larsson, P. Andersson, P. Blomqvist and B-E. Mellander, Nature Sci. Rep., 7 (2018) 10018, 13 pp. |
10. S. Chen, Z. Wang, J. Wang, X. Tong and W. Yan, J. Loss Prev. Process Ins., 63 (2020) 103992 7pp.
11. S. Bertilsson, F. Larsson, M. Furlani, I. Albinsson and B-E. Mellander, J. Power Sources, 373 (2018) 220 - 231.
12. A. R. Baird, E. J. Archibald, K. C. Marr and O. A. Ezekoye, J. Power Sources, 446 (2020) 227257, 13pp.
13. J. Roman, NFPA Journal January/February 2020. https://www.nfpa.org/News-and-Research/Publications-and-media/NFPA-Journal/2020/January-February-2020/Features/EV-Stranded-Energy.
14. McMicken Battery Energy Storage System Event Technical Analysis and Recommendations, Arizona Public Service, 18 July 2020. https://www.aps.com/-/media/APS/APSCOM-PDFs/About/Our-Company/Newsroom/McMickenFinalTechnicalReport.ashx?la=en&hash=50335FB5098D9858BFD276C40FA54FCE.
15. APS McMicken Progress Report, Exponent, 30 July 2020. https://docket.images.azcc.gov/E000007939.pdf.
16. M. B. McKinnon, S. DeCrane and S. Kerber, "Four Firefighters Injured In Lithium-Ion Battery Energy Storage System Explosion – Arizona", Underwriters Laboratories, 28 July 2020. https://ulfirefightersafety.org/posts/four-firefighters-injured-in-lithium-ion-battery-energy-storage-system-explosion.html
17. Tom Abbot Fire Chief of Surprise, Arizona Private Communication, 10 October 2019.
18. https://www.energy-storage.news/news/south-korea-fire-small-failures-shouldnt-lead-to-major-issues-dnv-gl-says.
19. http://www.businesskorea.co.kr/news/articleView.html?idxno=41012
20. https://www.brisbanetimes.com.au/national/queensland/firefighter-injured-in-overnight-blaze-at-griffith-university-campus-20200316-p54aet.html.
21. Report number IR201631f, Queensland Government, Incident at Griffith University, Nathan Campus, building N7, 24 April 2019.
22. X. Feng, M. Ouyang, X. Liu, L. Lu, Y. Xia and X. He, Energy Storage Mat., 10 (2018) 246 – 267.

This is the accepted version of this paper. Paper can be referenced as:
P. Christensen, Z. Milojevic, M.S. Wise, M. Ahmeid, P.S. Attidekou, W. Mrozik, N.A. Dickman, F. Restuccia, S.M.Lambert, P.K. Das. *Thermal and mechanical abuse of electric vehicle pouch cell modules*, Applied Thermal Engineering, 2021. https://doi.org/10.1016/j.applthermaleng.2021.116623

23. V. G. Choudhari, A. S. Dhoble and S. Panchal, Int. J. Heat and Mass Transfer, 163 (2020) 120434.
24. M. S. Patil, J. H. Seo, S. Panchal and M. Y. Lee, Int. J. Energy Research, 2020; 1 – 27.
25. J. Sun, J. Li, T. Zhu, K. Yang, S. Wei, N. Tang, N. Dang, H. Li, X. Qiu and L. Chen, Nano Energy, 27 (2016) 313 – 319.
26. H. Li, W. Peng, X. Yang, H. Chen, J. Sun and Q., Fire Technol., 56 (2020) 2545 – 2564.
27. L. Canals Casals, B. Amante García and C. Canal, J. Environ. Man., 232 (2019) 354 – 363.
28. J. Tebbit, N. Booth and J. Henderson, "A report on the likely mainstream technologies in the mid 2020's that SAP 11 will need to consider", SAP Industry Forum, 9 April 2020, p73. https://files.bregroup.com/SAP/SAP_11_Technologies_Report_Final_v2.0.pdf.
29. https://www.energy-storage.news/news/fire-at-20mw-uk-battery-storage-plant-in-liverpool.
30. https://www.statista.com/statistics/1011187/projected-global-lithium-ion-battery-market-size/.
31. C. J. Orendorff, Interface, Summer 2012, 61 – 65.
32. X. Feng, M. Fang, X. He, M. Ouyang, L. Lu, H. Wang, M. Zhang, J. Power Sources, 255 (2014) 294 – 301.
33. F. Larsson, S. Bertilsson, M. Furlani, I. Albinsson and B-E. Mellander, J. Power Sources, 373 (2018) 220 - 231.
34. G. Atkinson, J. Hall and A. McGillivray, Review of Vapour Cloud Explosion Incidents, HSE Research Report RR1113, 2017.
35. W. Zhao, G. Luo and C. –Y. Wang, J. Electrochem. Soc., 162 (2014) A207 – A217.
36. T. Yokoshima et al., J. Power Sources, 393 (2018) 67 - 74.
37. X. Feng, S. Zheng, X. He, L. Wang, Y. Wang, D. Ren and M. Ouyang, Frontiers En. Res., 6 (2018) 126, 16 pp.
38. X. Feng, S. Zheng, D. Ren, X. He, L. Wang, H. Cui, X. Liu, C. Jin, F. Zhang, C. Xu, H. Hsu, S. Gao, T. Chen, Y. Li, T. Wang, H. Wang, M. Li and M. Ouyang, Appl. Energy, 246 (2019) 53 – 64.
39. Z. Liao, S. Zhang, K. Li, M. Zhao, Z. Qiu, D. Han, G. Zhang and T. G. Habetler, J. Energy St., 27 (2020) 101065 9pp.
40 P. Ribière, S. Grugeon, M. Morcrette, S. Boyanov, S. Laruelle and G. Marlair, Energy Environ. Sci., 5 (2012) 5271 - 5280.
41. F. Larsson, P. Andersson, P. Blomqvuist and B-E. Mellander, Nature Sci. Rep., 7:10018 (2017), 13 pp.
42. F. Diaz, Y. Wang, R. Weyhe and B. Friedrich, Waste Management, 84 (2019) 102 – 111.
43. N. Warner, 2017. Overview of a year of battery fire overview of a year of battery fire testing by DNV GL for Con Ed, NYSERDA and FDNY 34. DNV GL, NFPA 855 Committee Meeting. https://nysolarmap.com/media/1743/n-warner_dnv-glbattery-testing-results.pdf. Accessed 26 May 2018.
44. DNV GL Maritime, "Technical Reference for Li-ion Battery Explosion Risk and Fire Suppression", Report No.: 2019-1025, 1 November 2019.
45. S. S. Zhang, J. Power Sources 162 (2006) 1379–1394.
46. A. Lecocq, G. G. Eshetu, S. Grugeon, N. Martin, S. Laruelle and G. Marlair, J. Power Sources 316 (2016) 197 - 206.
47. F. Ren, W. Zuo, X. Yang, M. Lin, L. Xu, W. Zhao, S. Zheng and Y. Yang, J. Phys. Chem. C 2019, 123, 10, 5871-5880.
48. P. Jankowski, N. Lindahl, J. Weidow, W. Wieczorek and P. Johansson, ACS Appl. En. Mat. 1(6) (2018) 2582 – 2591.
49. G. H. Wrodnigg, J. O. Besenhard and M. Winter, J. Power Sources 97-98 (2001) 592-594.
50. Wu, Z., Li, S., Zheng, Y., Zhang, Z., Umesh, E., Zheng, B., Zheng, X. and Yang, Y. J. Electrochem. Soc., 165(11) (2018) A2792 - A2800.

This is the accepted version of this paper. Paper can be referenced as:
P. Christensen, Z. Milojevic, M.S. Wise, M. Ahmeid, P.S. Attidekou, W. Mrozik, N.A. Dickman, F. Restuccia, S.M.Lambert, P.K. Das. *Thermal and mechanical abuse of electric vehicle pouch cell modules*, Applied Thermal Engineering, 2021. https://doi.org/10.1016/j.applthermaleng.2021.116623

51. V. Babrauskas, "Ignition handbook: principles and applications to fire safety engineering, fire investigation, risk management and forensic science." (2003), ISBN-10 : 0972811133.
52. A. Nedjalkov, J. Meyer, M. Köhring, A. Doering, M. Angelmahr, S. Dahle, A. Sander, A. Fischer, W. Schade, Batteries, 2 (2016) 5, 10pp.
53. D. P. Abraham, E. P. Roth, R. Kostecki, K. McCarthy, S. MacLaren and D. H. Doughty, J. Power Sources, 161 (2006) 648 - 657.
54. Y. Chen, N. Liu, Y. Jie, F. Hu, Y. Li, B. P. Wilson, Y. Xi, Y. Lai and S. Yang, ACS Sus. Chem. Eng. 7 (2019) 18228 - 18235.
55. T. Ohsaki, T. Kishi, T. Kuboki, N. Takami, N. Shimura, Y. Sato, M. Sekino and A. Satoh, J. Power Sources, 146 (2005) 97 - 100.
56. M. Onuki, S. Kinoshita, Y. Sakata, M. Yanagidate, Y. Otake, M. Ue and M. Deguchi, J. Electroch. Soc. 155 (2008) A794 – A797.
57. C. Essl, A. W. Golubkov, E. Gasser, M. Nachtnebel, A. Zankel, E. Ewert and A. Fuchs, Batteries, 6 (2020) 30, 28 pp.
58. A. O. Said, C. Lee, S. I. Stoliarov, J. Power Sources, 446 (2020) 227347, 14 pp.
59. A. W. Golubkov, S. Scheikl, R. Planteu, G. Voitic, H. Wiltsche, C. Stangl, G. Fauler, A. Thaler and V. Hacker, RSC Advances 5, (2015) 57171 - 57186.
60. P. Burgyniec, J. N. Davidson, D. J. Cummings and S. F. Brown, J. Power Sources, 414 (2019) 557 – 568.
61. X. Zhu, H. Wang, X. Wang, Y. Gao, S. Allu, E. Cakmak and Z. Wang, J. Power Sources, 455 (2020) 227939, 13 pp.
62. P. Balakrishnan, R. Ramesh and J. Kumar, J. Power Sources (2006) 155 (2006) 401 - 414.
63. A. Wang, S. Kadam, H. Li, S. Shi and Y. Qi, NPJ Nature Comput. Mater. 4 (2018) 15.
64. Z. Mao, M. Farkhondeh, M. Pritzker, M. Fowler and Z. Chen, (2017) J. Electrochem. Soc., 164 (2017) A3469 - A3483.
65. Q. Wang, J. Sun, X. Yao and C. Chen, J. Electrochem. Soc., 153(2) (2006) A329 – A333.
66. X. Feng, D. Ren, X. He and M. Ouyang, Joule, 4 (2020) 743 – 770.
67. Q-F. Yuan, F. Zhao, W. Wang, Y. Zhao, Z. Liang, D. Yan, Electrochim. Acta, 178 (2015) 682 – 688.
68. https://www.rsc.org/periodic-table/element/3/lithium
Y. Zhu, J. Xie and Y. Cui, Nature Commun., 10 (2019) 2067 7pp
70. X. Liu, D. Ren, H. Hsu, X. Feng, G-L. Xu, M. Zhuang, H. Gao, L. Lu, X. Han, Z. Chu, J. Li, X. He, K. Amine and M. Ouyang, Joule, 2 (2018) 2047 – 2064.
71. X. He, F. Restuccia, Y. Zhang, Z. Hu, X. Huang, J. Fang and G. Rein, Fire Technol., 56 (2020) 2649 – 2669.

This is the accepted version of this paper. Paper can be referenced as:
P. Christensen, Z. Milojevic, M.S. Wise, M. Ahmeid, P.S. Attidekou, W. Mrozik, N.A. Dickman, F. Restuccia, S.M.Lambert, P.K. Das. *Thermal and mechanical abuse of electric vehicle pouch cell modules*, Applied Thermal Engineering, 2021. https://doi.org/10.1016/j.applthermaleng.2021.116623

Thermal and mechanical abuse of electric vehicle pouch cell modules
Supplementary information

(a)

(b)

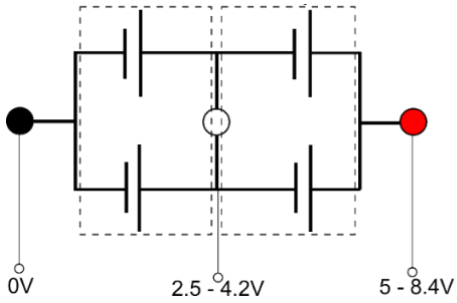

(c)

Figure S1. (a) The 8-cell module, (b) a pouch cell and (c) the wiring of the cells within the modules: the cells are arranged in two units of four cells with no connection between the units.

This is the accepted version of this paper. Paper can be referenced as:
P. Christensen, Z. Milojevic, M.S. Wise, M. Ahmeid, P.S. Attidekou, W. Mrozik, N.A. Dickman, F. Restuccia, S.M.Lambert, P.K. Das. *Thermal and mechanical abuse of electric vehicle pouch cell modules*, Applied Thermal Engineering, 2021. https://doi.org/10.1016/j.applthermaleng.2021.116623

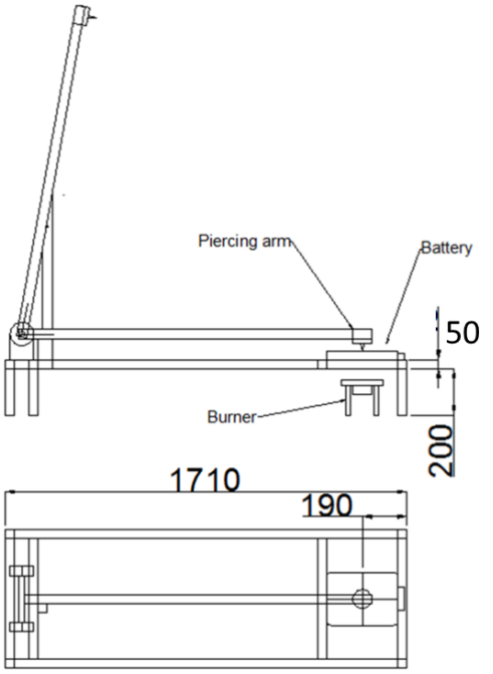

Figure S2. The frame employed to mount the modules for the ignition experiments. Measurements are in mm.

This is the accepted version of this paper. Paper can be referenced as:
P. Christensen, Z. Milojevic, M.S. Wise, M. Ahmeid, P.S. Attidekou, W. Mrozik, N.A. Dickman, F. Restuccia, S.M.Lambert, P.K. Das. *Thermal and mechanical abuse of electric vehicle pouch cell modules*, Applied Thermal Engineering, 2021. https://doi.org/10.1016/j.applthermaleng.2021.116623

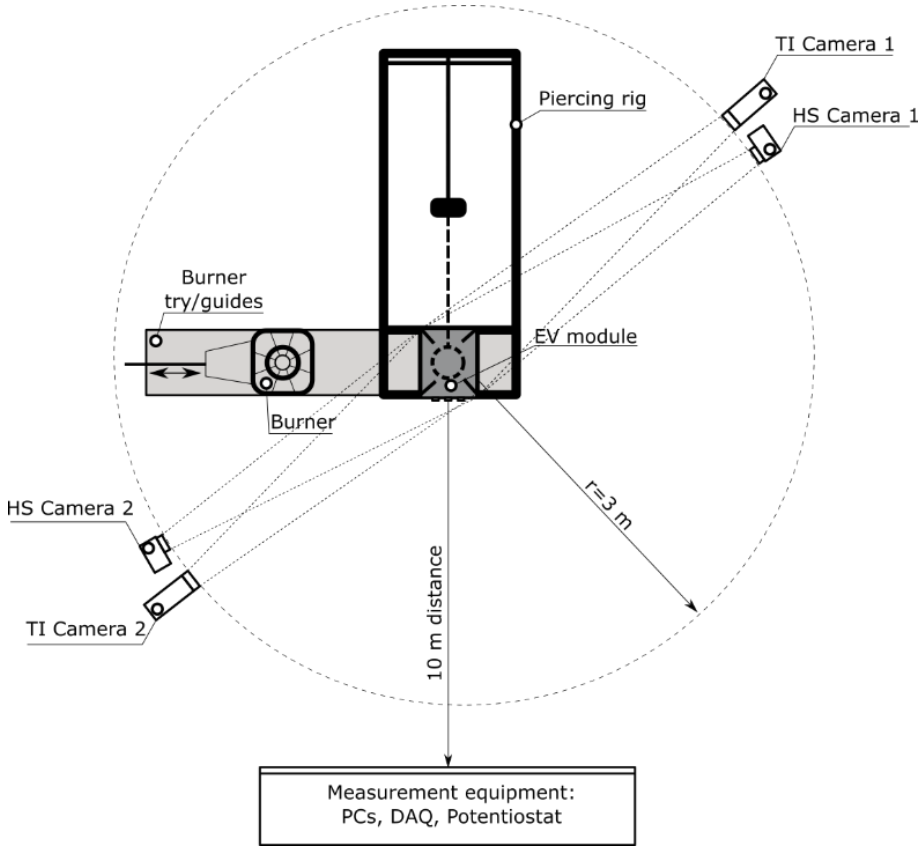

(a)

This is the accepted version of this paper. Paper can be referenced as:
P. Christensen, Z. Milojevic, M.S. Wise, M. Ahmeid, P.S. Attidekou, W. Mrozik, N.A. Dickman, F. Restuccia, S.M.Lambert, P.K. Das. *Thermal and mechanical abuse of electric vehicle pouch cell modules*, Applied Thermal Engineering, 2021. https://doi.org/10.1016/j.applthermaleng.2021.116623

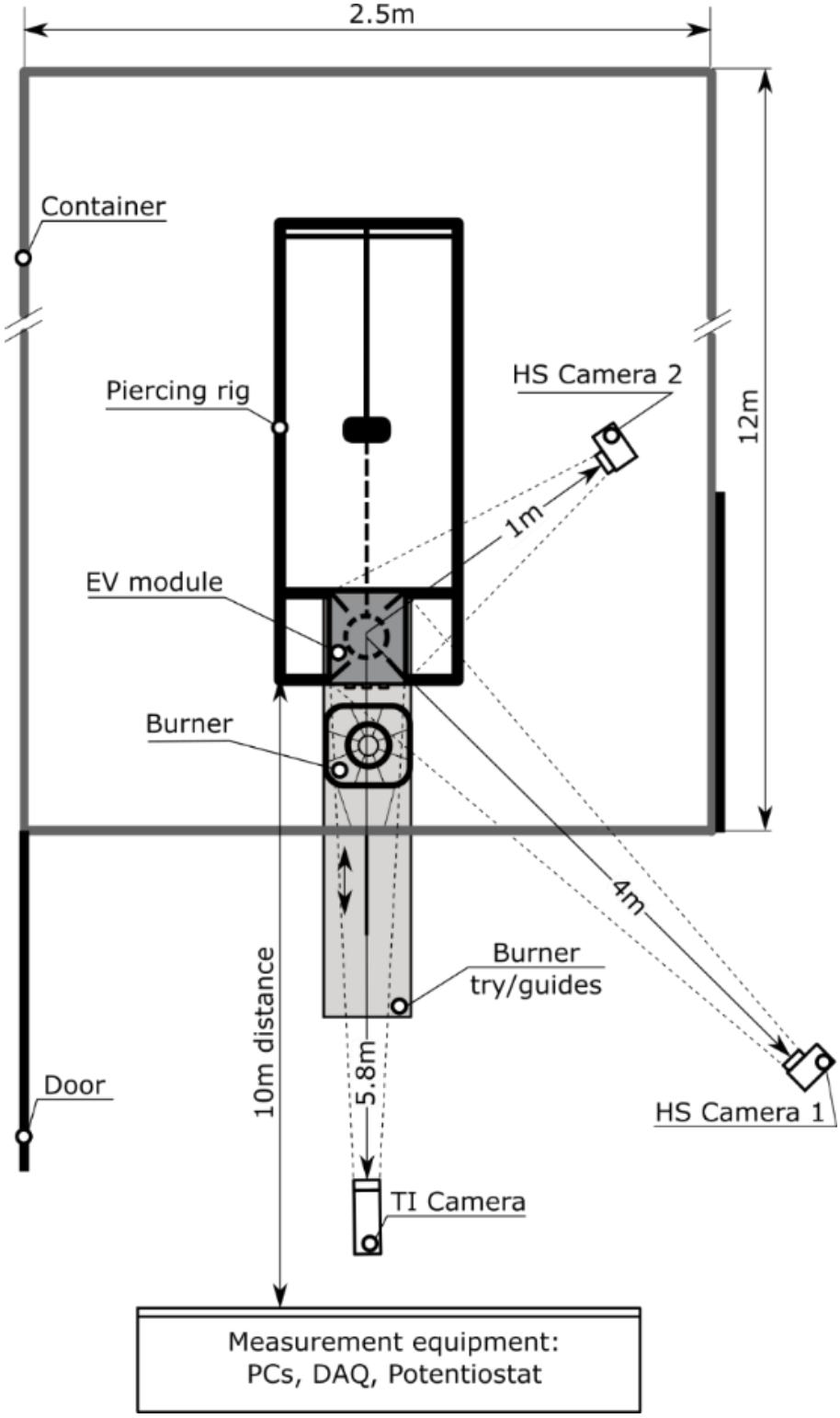

(b)

Figure S3. Positions of the module in the piercing rig, cameras and measurement equipment employed during the experiments at the (a) DNV GL and (b) FSC sites – as viewed from above

This is the accepted version of this paper. Paper can be referenced as:
P. Christensen, Z. Milojevic, M.S. Wise, M. Ahmeid, P.S. Attidekou, W. Mrozik, N.A. Dickman, F. Restuccia, S.M.Lambert, P.K. Das. *Thermal and mechanical abuse of electric vehicle pouch cell modules*, Applied Thermal Engineering, 2021. https://doi.org/10.1016/j.applthermaleng.2021.116623

The flame areas and lengths were calculated by image processing all the individual optical images in MATLAB. The values calculated from the front and rear camera for flame length and flame areas can differ, depending on the direction of particular flame flares, hence results from both cameras are presented in the results section, to try and account for different flare angles and directions.

A back camera was employed in the first FSC experiment: however, because the experiments were carried out inside a container the camera was destroyed at the end of the experiment as it could not be placed at a safe distance from the burning module. Hence, only a front camera was used in the two remaining experiments.

Flame lengths were calculated for all seven DNV GL experiments and experiments one and three at the FSC. FSC experiment two did not result in ignition and is therefore not included in this analysis.

For the flame length and area analyses, each optical image was converted into white/black pixels based on the presence of flame vs lack of flame. Figure S4 shows data from DNV GLS experiment two as an example of the image processing of the stills for calculations of flame length and areas from both the front and back cameras. As can be seen from the images, the processing clearly identifies the flames while keeping the battery pack a fixed black colour (centre of images in (b) and (d)) and removes effects from reflections, as can be seen by comparing the images in (c) and (d).

(a)

(b)

This is the accepted version of this paper. Paper can be referenced as:
P. Christensen, Z. Milojevic, M.S. Wise, M. Ahmeid, P.S. Attidekou, W. Mrozik, N.A. Dickman, F. Restuccia, S.M.Lambert, P.K. Das. *Thermal and mechanical abuse of electric vehicle pouch cell modules*, Applied Thermal Engineering, 2021. https://doi.org/10.1016/j.applthermaleng.2021.116623

(c) *(d)*

Figure S4. Optical (a) and (c) and processed (b) and (d) images for the calculation of flame length from (a) the back camera and (c) the front camera.

With multiple data sets, a common start time is difficult to identify. To achieve this, the frames of the thermal videos were extracted using VLC and a significant event selected, e.g. burner ignition see Figure S5. The corresponding frame from the optical images was then identified and selected, see Figure S6, and hence the timing of the images could then be correlated in absolute terms.

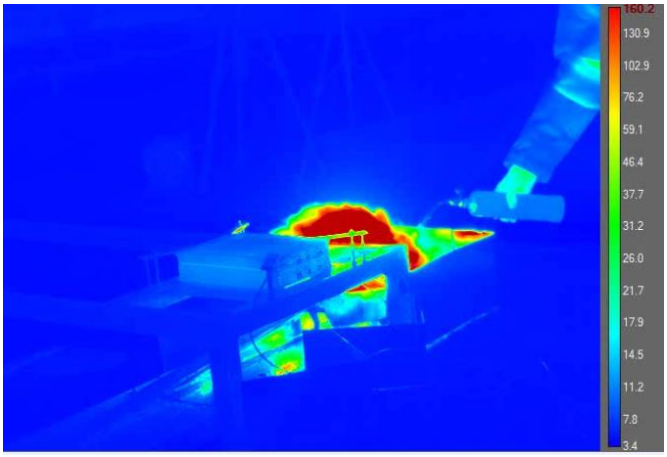

Figure S5. Thermal image showing the lighting of the burner being lit at RAFS.

Figure S6: The optical image equivalent of figure S5.

<u>This is the accepted version of this paper. Paper can be referenced as:</u>
P. Christensen, Z. Milojevic, M.S. Wise, M. Ahmeid, P.S. Attidekou, W. Mrozik, N.A. Dickman, F. Restuccia, S.M.Lambert, P.K. Das. *Thermal and mechanical abuse of electric vehicle pouch cell modules*, Applied Thermal Engineering, 2021. https://doi.org/10.1016/j.applthermaleng.2021.116623

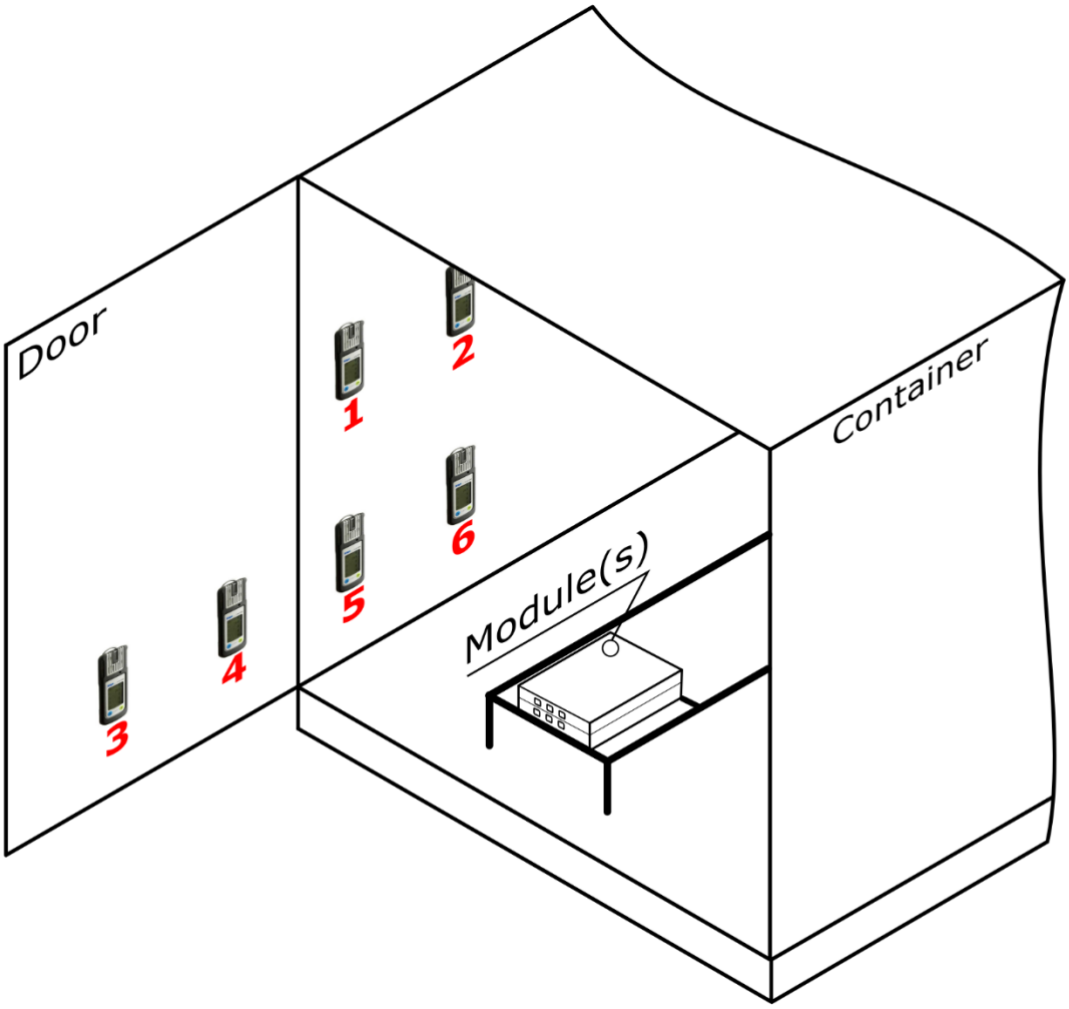

Figure S7. Schematic showing the locations of the gas sensors in the Fire Services College experiments.

This is the accepted version of this paper. Paper can be referenced as:
P. Christensen, Z. Milojevic, M.S. Wise, M. Ahmeid, P.S. Attidekou, W. Mrozik, N.A. Dickman, F. Restuccia, S.M.Lambert, P.K. Das. *Thermal and mechanical abuse of electric vehicle pouch cell modules*, Applied Thermal Engineering, 2021. https://doi.org/10.1016/j.applthermaleng.2021.116623

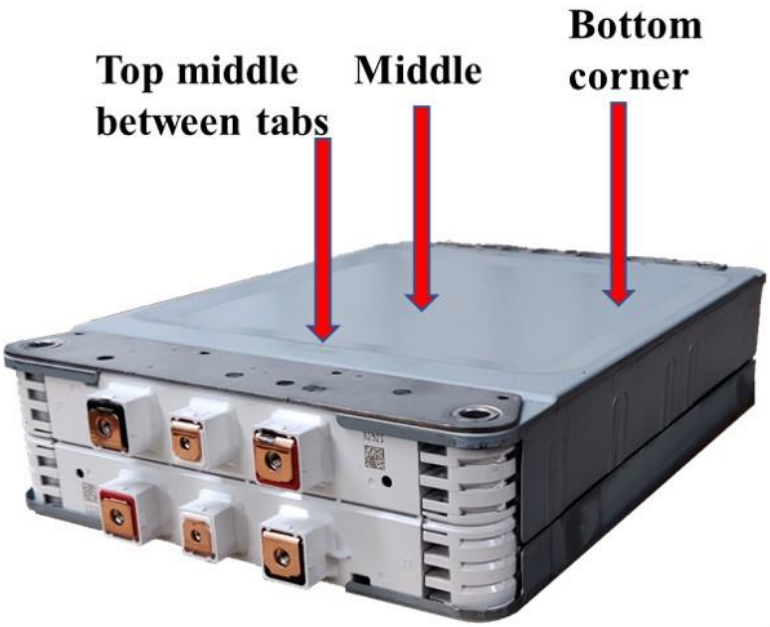

Figure S8. The location of the nail penetrations in experiments 2 to 4 at the DNV GL site.

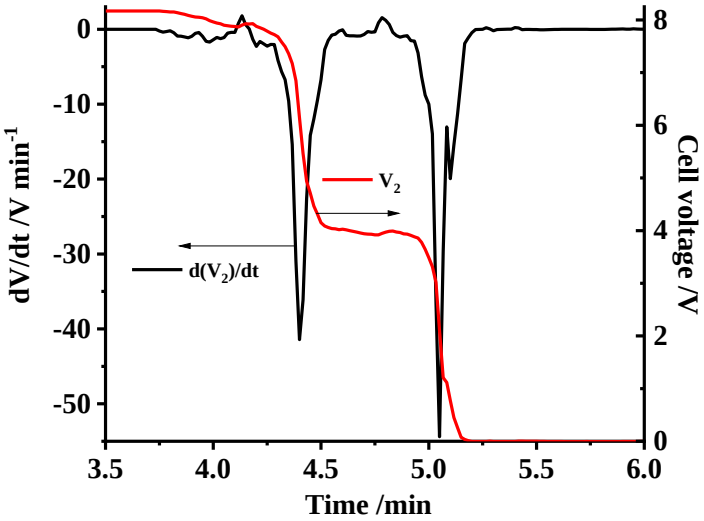

Figure S9. The voltage of the cells of the top quartet of the module, V2, in Figures 12(a) and (b) and the first derivative of the same recorded during the burner experiment, experiment 1.

This is the accepted version of this paper. Paper can be referenced as:
P. Christensen, Z. Milojevic, M.S. Wise, M. Ahmeid, P.S. Attidekou, W. Mrozik, N.A. Dickman, F. Restuccia, S.M.Lambert, P.K. Das. *Thermal and mechanical abuse of electric vehicle pouch cell modules*, Applied Thermal Engineering, 2021. https://doi.org/10.1016/j.applthermaleng.2021.116623

Figure S10. Photograph of the underside of the module employed in experiment 2 at the DNV GL site showing the exit hole (arrowed) of the nail.

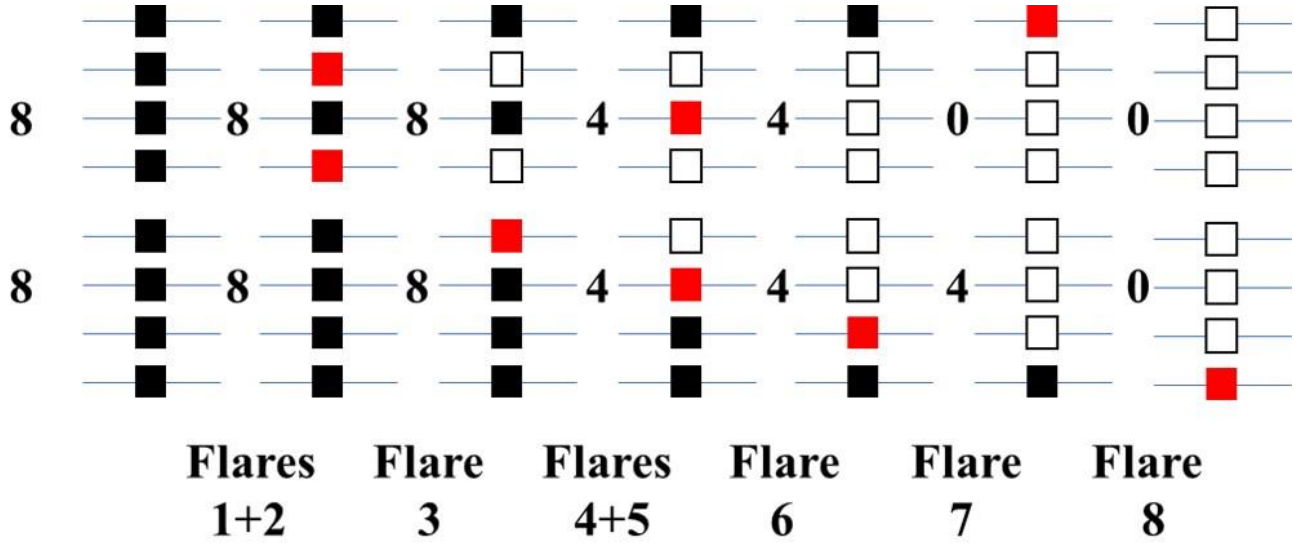

Figure S11. The failure of the individual cells of the module during experiment 2 at the DNV GL site, based on the voltage and flame area data in Figure 7(c). Black cells are undamaged, red cells have failed as a result of the previous flare and white cells are dead. Numbers refer to the measure voltages: top V2 and bottom V1.

This is the accepted version of this paper. Paper can be referenced as:
P. Christensen, Z. Milojevic, M.S. Wise, M. Ahmeid, P.S. Attidekou, W. Mrozik, N.A. Dickman, F. Restuccia, S.M.Lambert, P.K. Das. *Thermal and mechanical abuse of electric vehicle pouch cell modules*, Applied Thermal Engineering, 2021. https://doi.org/10.1016/j.applthermaleng.2021.116623

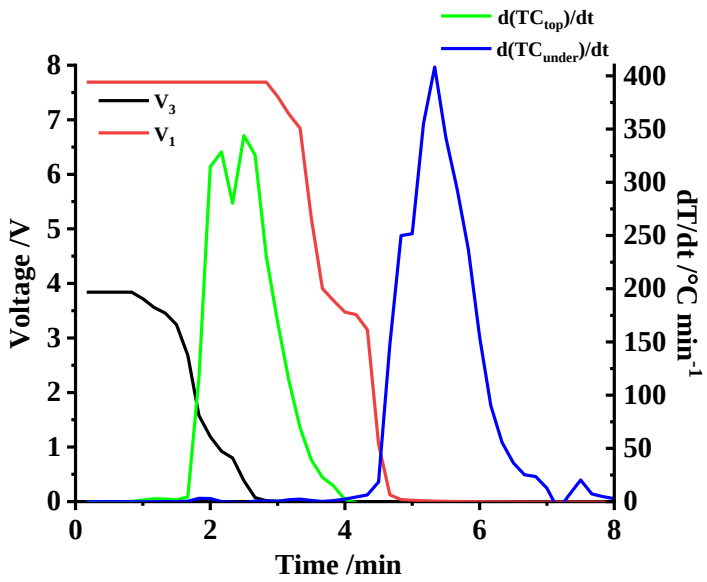

Figure S12. Voltage data and the first derivatives of the thermocouple data in Figure 13.

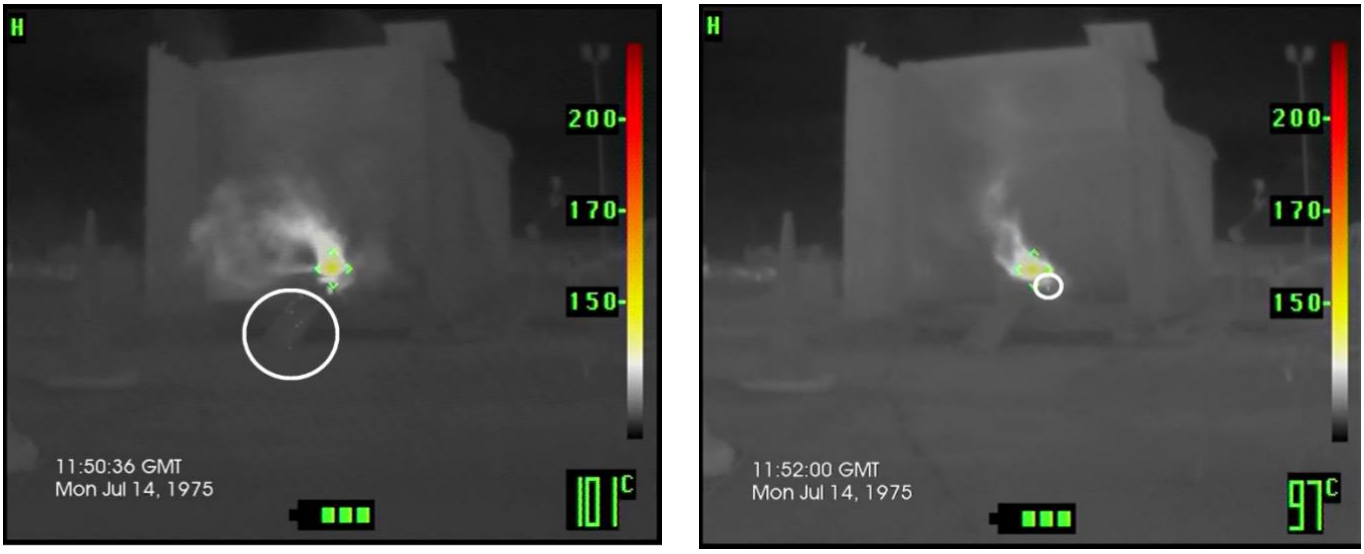

(a) *(b)*

Figure S13. Thermal images collected (a) 106 s and (b) 189 s after nail penetration in experiment 2 at the FSC site.

This is the accepted version of this paper. Paper can be referenced as:
P. Christensen, Z. Milojevic, M.S. Wise, M. Ahmeid, P.S. Attidekou, W. Mrozik, N.A. Dickman, F. Restuccia, S.M.Lambert, P.K. Das. *Thermal and mechanical abuse of electric vehicle pouch cell modules*, Applied Thermal Engineering, 2021. https://doi.org/10.1016/j.applthermaleng.2021.116623